Canadian Geotechnical Journal

Research Article

Long-term performance of textured HDPE geomembranes in municipal solid waste landfills

R. Kerry Rowe[a], **M.M. Ali**[b], **and M.S. Morsy**[c]

[a]Geotechnical and Geoenvironmental Engineering, GeoEngineering Centre at Queen's-RMC, Queen's University, Ellis Hall, Kingston, ON K7L 3N6, Canada; [b]GeoEngineering Centre at Queen's-RMC, Queen's University, Kingston, ON K7L 3N6, Canada; [c]Soil Mechanics and Foundation Engineering Unit, Structural Engineering Department, Faculty of Engineering, Ain Shams University, Cairo 11535, Egypt

Corresponding author: **R. Kerry Rowe** (email: kerry.rowe@queensu.ca)

Abstract

The effect of blown-film co-extrusion texturing (using entrained nitrogen gas) on the long-term performance of high-density polyethylene geomembranes (GMBs) immersed in synthetic municipal solid waste leachate is examined over an approximately 8-year period. Antioxidant depletion of the textured part is shown to be much faster than that of the smooth edge. Likewise, the degradation in the tensile break properties at 85 °C is faster for the textured part than for the smooth-edge portion and smooth equivalent. The updated estimates for antioxidant depletion time based on data at four different temperatures (40, 55, 75, and 85 °C) over 98 months of data collection are compared with predictions based on 34 months of data, and the implications are discussed. Nominal failure was reached at 75 °C, and this combined with data at 85 °C allows prediction of the time between depletion of standard oxidative induction time and nominal failure at lower temperatures. The effect of salt concentration in incubation fluid on the time to degradation is examined. Finally, the paper comments on the uses of textured versus smooth GMB.

Key words: textured geomembranes, stress crack resistance, mechanical properties, municipal solid waste landfills, degradation, antioxidant depletion.

1. Introduction

High-density polyethylene (HDPE) geomembranes (GMBs) play an essential role in various geoenvironmental barrier systems, as they serve to contain liquids and gases with a design life that spans from decades to millennia (Giroud and Bonaparte 1989; Rowe et al. 1998, 2004, 2020; Rowe and Sangam 2002; Sangam and Rowe 2002; Rowe 2005; Abdelaal et al. 2014*b*, 2023*a*, 2023*b*; Ewais and Rowe 2014; Morsy and Rowe 2017, 2020*a*; Clinton and Rowe 2023; Rowe and Somuah 2023; Zafari et al. 2023*a*, 2023*b*, 2024). HDPE GMBs are prone to various degradation mechanisms when exposed to long-term field exposure conditions (Rowe and Sangam 2002; Hsuan et al. 2008; Scheirs 2009), resulting in a reduction in both their mechanical and physical properties (Rowe 2005, 2020; Abdelaal et al. 2014*a*). The oxidative degradation of a GMB consists of three conceptual stages (Hsuan and Koerner 1998): Stage I, the depletion of antioxidants assessed by oxidative inductive time; Stage II, the induction period to the onset of polymer degradation; and Stage III starts when polymer degradation occurs resulting in a measurable reduction in GMB properties such as tensile properties (ASTM 2020*b*), melt flow index (MFI; ASTM 2013), and stress crack resistance (SCR; ASTM 2020*a*). The time to nominal failure of the GMB is reached when its mechanical and physical properties decrease to 50% of the initial (Rowe et al. 2009) or specified value (e.g., those given in GRI-GM13 2019).

More recent studies have shown that degradation of mechanical properties of a GMB could occur before full depletion of antioxidants due to physical aging (Ewais and Rowe 2014; Rowe et al. 2019; Morsy and Rowe 2020*a*) in which the SCR decreased to an equilibrium stress crack resistance (SCR_m) value, or excessive surface degradation (i.e., connected network of cracks on the unnotched surface) (Abdelaal et al. 2019; Morsy et al. 2021). Therefore, the time to nominal failure could be defined as the time at which the SCR degrades to 50% of SCR_m, the stabilized value of SCR after physical aging and stress relaxation (Rowe et al. 2019; Morsy and Rowe 2020*a*).

Texturing the surface of GMBs is used to increase the interface friction between the GMB and soil or geosynthetic liners with which they are in contact (Koerner 2005; Müller 2007; Scheirs 2009). This texturing enhances the interaction between the GMB and the material it contacts, thereby improving the veneer stability of the lining system on side slopes. Texturing can be applied to one or both surfaces of the GMBs with the blown-film process, which is typically achieved by injecting an inert gas, such as nitrogen, into the molten plastic of the outer layer(s) during the extrusion process. As the plas-

tic exits the die, the gas cools and ruptures within the skin layers, creating a textured surface. While this co-extrusion method provides greater interface friction at low normal stresses compared to other techniques (e.g., spray-on texturing and pattern texturing; Erickson et al. 2008), it also causes variability in the core thickness of the GMB. Consequently, this may result in a large coefficient of variation in the material's mechanical properties due to the stress concentrations between the asperities (Rowe et al. 2020). While the variability in tensile properties is not directly relevant to field performance since the strains are to be kept well below the yield strain, the cause of the variability in tensile properties ultimately manifests itself in variability in SCR and a decrease in performance of unnotched textured specimens compared to smooth specimens from the edge of same roll as will be discussed in more detail in a later section. Evaluating the SCR of textured blown-film GMBs presents significant challenges but, as demonstrated by Abdelaal et al. (2024), it can be achieved. Textured GMB rolls commonly have a smooth-edge portion to facilitate welding in the field. Several studies have examined the longevity of black smooth HDPE GMBs under various exposure conditions (Mueller and Jakob 2003; Rowe et al. 2009; Abdelaal and Rowe 2014, 2017; Rowe and Ewais 2014; Rowe and Shoaib 2017; Tian et al. 2017; Ewais et al. 2018; Abdelaal et al. 2019, 2023*a*; Morsy et al. 2021). However, only a few studies have explored the effect of texturing on aging of HDPE GMBs in recent research (Morsy and Rowe 2020*a*).

Morsy and Rowe (2020*a*) examined the long-term behaviour of a 1.5 mm thick black textured GMB and its smooth edge when immersed in a simulated synthetic municipal solid waste (MSW) leachate at four different temperatures. Based on results over 3 years of incubation, they found that the antioxidant depletion time for the textured portion was 40% faster for standard oxidative induction time (Std-OIT) and 9% faster for the high-pressure oxidative induction time (HP-OIT) compared to the smooth edge, suggesting that the texturing affected the antioxidant depletion stage. The SCR results indicated that the texturing resulted in a relatively small difference in the time to nominal failure between the textured portion and its smooth edge at 85 °C, leaving a question about its performance at lower temperatures (e.g., 75 °C). Recent research has shown that the difference in the core thickness of the textured and smooth-edge portions of a textured GMB leads to differences in the degradation time and behaviour of the two portions (Zafari et al. 2023*a*). However, the textured and smooth portions in that study (Zafari et al. 2023*a*) were not identical, unlike the current study where both the textured and smooth portions are made from exactly the same resin and stabilized with the same antioxidant package (e.g., similar initial Std-OIT and HP-OIT; Table 1). Therefore, the result of the current study allows consideration of the effect of texturing on the longevity of a GMB with minimal uncertainty due to other contributing factors.

The only studies of the effects of texturing on aging are for 3 years (Morsy and Rowe 2020*a*) and 5 years (Zafari et al. 2023*b*). While the three GMBs studied all reached nominal failure in 3 years at 85 °C, nominal failure was not reached at 75 °C for any GMB, and so it was only possible to assess the effect of texturing on Stage I over a range of temperatures (Morsy and Rowe 2020*a*). This leaves a major uncertainty regarding the effect of texturing on stages II and III to nominal failure. Thus, the objective of this study is to continue the study of Morsy and Rowe (2020*a*) with an additional 5 years (total 8 years) of incubation in synthetic MSW leachate and investigate the behaviour of the textured HDPE GMBs and their smooth edges. The objectives of this study are to

1. Investigate the performance of a textured black HDPE GMB and its smooth edge in synthetic MSW leachate and compare them with an "equivalent smooth" GMB made from the same nominal resin to enhance the prediction of the Std-OIT and HP-OIT depletion time at temperatures $\leq$ 55 °C by adding 60 months of data to the findings in Morsy and Rowe (2020*a*).
2. Examine the effect of texturing on the longevity of the HDPE GMB by comparing the time to nominal failure, t_{NF}, based on tensile break strain and strength of the textured and smooth-edge portions and compare with the results for SCR and high-load melt index (HLMI) at 85 °C reported by Morsy and Rowe (2020*a*).
3. Investigate the t_{NF} based on SCR for textured and smooth-edge portions of the textured GMB and the smooth equivalent to the textured GMB at 75 °C.
4. Use the available data at 75 and 85 °C to establish an Arrhenius relationship for the length of stages II and III to nominal failure and examine the implications of this information.
5. Investigate the effect of the presence and absence of salts in the leachate on SCR, tensile properties, and HLMI after 80-month immersion at 85 °C.

2. Experimental investigation

2.1. GMBs examined

Both textured and smooth black HDPE GMBs examined (Table 1) were manufactured from the same medium-density polyethylene nominal resin (Chevron Marlex PE K306) in 2015. The textured GMB (denoted as *MxTA15*) was produced by co-extrusion with a blowing agent and had an average core thickness of 1.5 $\pm$ 0.04 mm and an average asperity height of 0.43 mm. The average thickness of the smooth edge of the textured GMB (denoted as *MxTsA15*) was 2.6% larger at 1.54 $\pm$ 0.01 mm, and the smooth "equivalent" GMB (denoted as *MxF15*) was midway between the texted and smooth edge averages at 1.52 $\pm$ 0.01 mm. Given the standard deviations indicated by $\pm$, there was no statistically significant difference in the core thickness of the three GMBs.

2.2. Immersion testing

The GMB coupons (190 mm $\times$ 95 mm) were incubated in 4 L glass jars filled with simulated synthetic MSW leachate (denoted as MSW-L3). To accelerate the aging of the GMBs, the jars were placed in forced air ovens at temperatures of 40, 55, 75, and 85 °C (maximum variation = $\pm$0.5 °C). The MSW-L3 leachate used (electrical potential, Eh $\approx$ −120 mV, total dissolved solids $\approx$ 12 000 mg/L, and pH $\approx$ 7; full details are given by Rowe et al. (2008) and Abdelaal et al. (2014*b*)) was prepared

Table 1. Initial properties of geomembranes (GMBs).

Property	Method	Unit	Mean ± SD[a]		
GMB	–	–	Textured	Smooth edge	Smooth
Designator	–	–	*MxTA15*	*MxTsA15*	*MxF15*
Type	–	–	HDPE	HDPE	HDPE
Thickness	–	mm	1.5 ± 0.04	1.54 ± 0.01	1.52 ± 0.01
			ASTM D5994[c]	ASTM D5199[d]	ASTM D5199[d]
Asperity height	ASTM D7466[e]	mm	0.43	–	–
GMB density[b]	ASTM D1505[f]	g/cm^3	0.947	0.947	0.947
Std-OIT	ASTM D3895[g]	min	185 ± 10	185 ± 10	153 ± 6
HP-OIT	ASTM D5885[h]	min	1580 ± 90	1580 ± 90	990 ± 140
HLMI (21.6 kg)		g/10 min	13.3 ± 0.5	13.3 ± 0.5	15.3 ± 0.3
LLMI (2.16 kg)	ASTM D1238[i]	g/10 min	0.11 ± 0.002	0.11 ± 0.002	0.135 ± 0.002
Melt flow ratio		unitless	120.9 ± 2.4	120.9 ± 2.4	113.3 ± 0.5
SCR	ASTM D5397[j]	hours	1600 ± 1640	3970 ± 1020	3860 ± 700
			(150–5700)[l]	(2700–5700)[l]	(3100–4800)[l]
Tensile properties	ASTM D6693[k]	–	–	–	–
Break stress-cross machine direction	Type IV	kN/m	30.5 ± 1	28.6 ± 1	28.3 ± 1
Break strain-cross machine direction		%	35.3 ± 2	59 ± 4.5	55.2 ± 2.34
Break stress-cross machine direction	Type V	kN/m	38.5 ± 4	61 ± 2	58.5 ± 2
Break strain-cross machine direction		%	502 ± 41	784 ± 44	796 ± 13

Note: GMB, geomembrane; Std-OIT, standard oxidative induction time; HP-OIT, high-pressure oxidative induction time; HLMI, high-load melt index; LLMI, low-load melt index; SCR, stress crack resistance; HDPE, high-density polyethylene.
[a]Standard deviation.
[b]Provided by the manufacturer.
[c]ASTM (2010*a*).
[d]ASTM (2012).
[e]ASTM (2010*b*).
[f]ASTM (2010*c*).
[g]ASTM (2019).
[h]ASTM (2021).
[i]ASTM (2013).
[j]ASTM (2020*a*).
[k]ASTM (2020*b*).
[l](minimum–maximum).

using distilled water mixed with organic/inorganic salts, surfactant, reducing agent, and trace metal solution based on the chemical analysis of Keele Valley landfill MSW leachate in Ontario, Canada (Rowe et al. 2008). The GMB coupons were separated using 5 mm thick glass rods to ensure the exposure of GMBs to the MSW leachate from both sides. A limited number of tests were performed with leachate MSW-L5 prepared using the same distilled water mixed with surfactant, reducing agent, and trace metal solution as used for MSW-L3 but without the organic/inorganic salts (Abdelaal et al. 2014*b*). The leachate was replaced with fresh leachate every 2 months to control the concentration of synthetic MSW leachate during the immersion period (Abdelaal et al. 2014*b*).

2.3. Index testing

The depletion of different antioxidant packages was monitored using Std-OIT (35 kPa/200 °C; ASTM 2019) to detect hindered phenols and phosphite antioxidants, while the HP-OIT (150 °C, 3500 kPa; ASTM 2020*c*) was conducted to detect thiosynergists and hindered amine (light) stabilizers (HALS also known as HAS). The oxidative induction time (OIT) bore-cut specimens were prepared without homogenization (ASTM 2021) because the GMBs examined were smooth and textured black nonconductive GMBs. Homogenization is required only when the specimen is a multilayered GMB to minimize local variations in stabilizer concentration (ASTM 2021). Even in the case of multilayered GMBs, Zafari et al. (2023*a*, 2023*b*, 2024) demonstrated that while homogenization did affect the absolute value of OIT, the ratio of OIT at a given time, *t*, to the initial OITo indicated changes in behaviour at the same time irrespective of the method of testing adopted. The degradation in physical and mechanical properties of the GMBs was monitored using (1) single point notched constant tensile load (SP-NCTL; ASTM 2020*a* appendix) to evaluate the SCR, (2) HLMI (21.6 kg/190 °C; ASTM 2013), and (3) tensile properties (Type V; ASTM 2020*b*). The HLMI test was used to assess the changes in molecular weight distribution of the polymer to infer degradation by either cross-linking or chain-scission mechanisms (Hsuan and Koerner 1998). To monitor the degradation in the tensile break properties, tensile tests were conducted in cross-machine (XD) directions using smaller dog bone Type V specimens (ASTM 2014) at a displacement rate of 50 mm/min.

The SP-NCTL test was used to monitor physical aging and/or polymer degradation. SCR specimens from both the smooth edge and the smooth equivalent GMB, which are made from

the same nominal resin as the textured GMBs, were cut in the XD direction of the roll. These specimens were notched, leaving a consistent ligament thickness equal to 80% of the nominal thickness of the GMB (i.e., 1.2 mm). Subsequently, the notched specimens were incubated in a 10% IGEPAL solution at 50° C under applied stress equal to 30% of the yield strength (in kN/m) measured for their unaged counterparts (both smooth and smooth-edge GMBs). The IGEPAL solution is used to accelerate the SP-NCTL test. The stress cracking agent (IGEPAL® CO-630) diffuses through the polymer and plasticizes the amorphous zone, leading to faster softening and disentanglement of the fibrils.

With textured GMB, it was challenging to maintain a consistent ligament thickness of 1.2 mm in the textured GMBs due to the variation in ligament thickness of the notched specimens, resulting from nonuniform core thickness. Although GRI-GM13 (2019) does not recommend the use of SP-NCTL tests for textured GMBs, Morsy and Rowe (2020*a*) proposed using SP-NCLT tests to monitor the texturing effect on the time to nominal failure (t_{NF}) and assessing the physical aging of the GMB. For the aged textured GMB specimens, each specimen was inspected and specimens with a thickness variability exceeding 0.05 mm (4%) were rejected (as recommended by Morsy and Rowe (2020*a*)).

The index tests have shown that the initial Std-OIT, HP-OIT, and MFI for the textured and smooth-edge portions of the textured GMB were similar (Table 1). Thus, it can be inferred that the difference between the longevity of the textured portion and its smooth-edge counterpart was due to the co-extrusion texturing.

3. Results and discussion

3.1. Antioxidant depletion

3.1.1. Std-OIT depletion

The Std-OIT depletion data for the textured GMB (*MxTA15*), its smooth edge (*MxTsA15*), and the smooth equivalent GMB (*MxF15*) were fitted using a single two-parameter exponential decay function (Hsuan and Koerner 1998; Sangam and Rowe 2002; Rowe et al. 2009, 2020; Abdelaal et al. 2014*b*; Morsy and Rowe 2017) given by

$$\text{OIT}_t = \text{OIT}_0 e^{-st} \quad (1)$$

and taking the natural logarithm on both sides,

$$\ln(\text{OIT}_t) = \ln(\text{OIT}_0) - st \quad (2)$$

where OIT_t (min) is the Std-OIT value at time t, s (month^{-1}) is the antioxidant depletion rate, OIT_o (min) is the initial and, implicitly, $\text{OIT}_o = 0$ the final Std-OIT values.

In addition to the 34-month-aged specimens reported by Morsy and Rowe (2020*a*), Fig. 1 shows the depletion of Std-OIT at 40 and 55 °C in MSW-L3 after adding 64 months of data. For all examined GMBs, the Std-OIT depleted to a value of approximately $\text{OIT}_d = 3$ min at all incubation temperatures except 40 °C, which was still depleting after 8 years. The depletion rate of the textured GMB was faster compared to its smooth edge at all incubation temperatures (Figs. 1 and 2). The difference in the Std-OIT depletion between the textured and its smooth edge can be attributed to the difference in the core thickness (Table 1) and surface area. The texturing on the GMB surface results in an increase in the surface area of the GMB and allows a greater area through which antioxidants can diffuse or be extracted (Morsy and Rowe 2017). The variability in the core thickness of the textured GMB attributed to the co-extrusion process may have resulted in nonuniform shorter outward diffusion paths for the antioxidants, leading to shorter paths for antioxidants to migrate from the GMB core (Rowe et al. 2013*a*; Rowe and Ewais 2014). Consequently, the textured portion shows faster depletion rates relative to the smooth edge (other things being equal).

Although the textured and smooth equivalent GMB were made from the same nominal resin (Morsy and Rowe 2020*a*), the initial Std-OIT of the textured roll was notably (21%) higher than that of the smooth roll (Table 1). Whether this was happenstance or intended to enhance the long-term performance of the textured GMB is unclear. This may also support the hypothesis that the textured HDPE GMB should be boosted OIT by the manufacturer compared to the smooth to compensate for losses due to increased area for depletion. The full depletion of antioxidants was observed (Table 2) after ≈ 54 months at 55 °C, 8 months at 75 °C, and 3 months at 85 °C (Figs. 1 and 2) for the textured portion of the roll (*MxTA15*). For the smooth-edge portion of the roll, full depletion of antioxidants was observed after ≈ 64 months at 55 °C, 12 months at 75 °C, and 4 months at 85 °C (Figs. 1 and 2; *MxTsA15*). For the smooth equivalent roll, full depletion of antioxidants was observed after about 60 months at 55 °C, 8 months at 75 °C, and 3 months at 85 °C (Figs. 1 and 2) (*MxF15*). The antioxidant depletion rates (in month^{-1}) for the smooth roll and the smooth edge and textured portions of the textured roll (Fig. 2) were 0.007, 0.0051, and 0.0063 at 40 °C, 0.076, 0.065, and 0.065 at 55 °C, 0.53, 0.33, and 0.48 at 75 °C, and 1.51, 1.074, and 1.421 at 85 °C (Table 2), with the textured rate being consistently higher than the smooth edge by an average of 33%.

At temperatures of 55 and 75° C, the oxidation rate may differ significantly between the three GMBs due to variations in their surface area, core thickness, and presence of additives or texturing, affecting how antioxidants are consumed. However, at the higher temperature of 85° C, the oxidation rate increases to the point where the physical loss by extraction becomes the dominant factor (Scheirs 2009). At such elevated temperatures, antioxidants may rapidly diffuse to the surface and volatilize or get extracted.

3.1.2. HP-OIT depletion

Antioxidant depletion was monitored using HP-OIT test to detect antioxidants/stabilizers. Single three-parameter (OIT_0, s, and OIT_r) exponential decay function was used to fit the data viz:

$$\text{OIT}_t = \left[(\text{OIT}_0 - \text{OIT}_r)\, e^{-st}\right] + \text{OIT}_r \quad (3)$$

Fig. 1. Variation of the normalized standard oxidative induction time (Std-OIT) (OIT_t/OIT_0) with incubation time for the textured geomembrane (GMB), its smooth edge, and equivalent smooth GMB (*MxTA15*, *MxTsA15*, and *MxF15*) immersed in municipal solid waste leachate 3: (*a*) 40 °C (*MxTA15* and *MxTsA15*); (*b*) 40 °C (*MxF15* and *MxTsA15*); (*c*) 55 °C (*MxTA15* and *MxTsA15*); and (*d*) 55 °C (*MxF*15 and *MxTsA15*). Error bars represent the range of results.

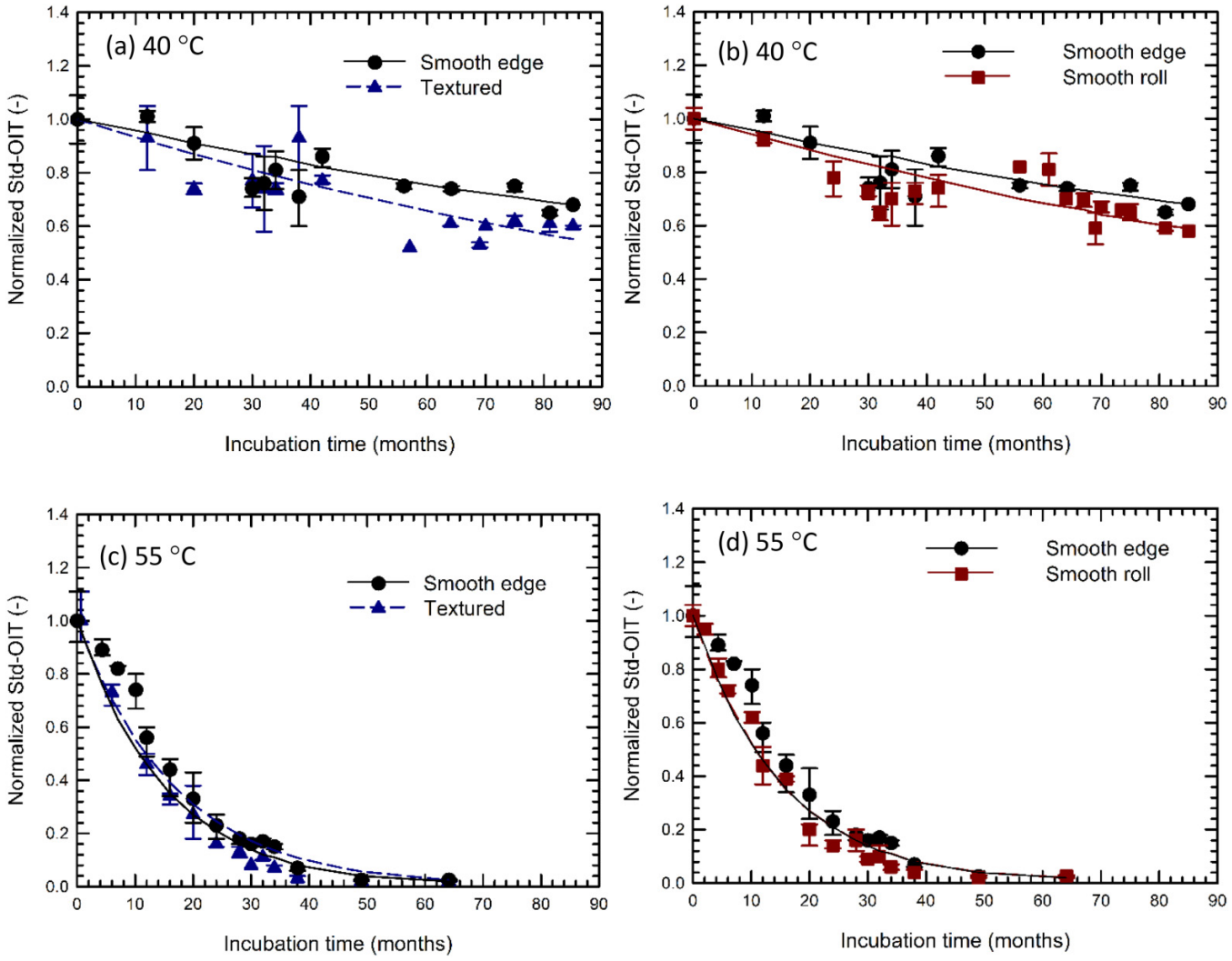

where OIT_t (min) is the HP-OIT value at time t, s ($month^{-1}$) is the antioxidant depletion rate, OIT_0 (min) is the initial HP-OIT value, and OIT_r (min) is the residual HP-OIT value.

With the addition of 64 months of data to that published by Morsy and Rowe (2020*a*), the full depletion of HP-OIT to residual values was observed for all the GMBs examined at all incubation temperatures except 40 °C during 98 months of incubation (Fig. 3).

The HP-OIT residual values for the textured, smooth edge, and smooth equivalent GMBs were 348, 630, and 238 at 55 °C, 220, 220, and 198 at 75 °C, and 220, 220, and 198 min at 85 °C, with normalized values (i.e., HP-OIT residual value divided by the initial HP-OIT value) of 0.22, 0.4, and 0.24 at 55 °C, 0.14, 0.14, and 0.2 at 75 °C, and 0.14, 0.14, and 0.2 at 85 °C. The observed depletion rates (in mo^{-1}) for *MxTA15*, *MxTsA15*, and *MxF15* were 0.014, 0.013, and 0.009 at 40 °C, 0.036, 0.037, and 0.034 at 55 °C, 0.095, 0.08, and 0.085 at 75 °C, and 0.389, 0.304, and 0.251 at 85 °C (Figs. 4 and 5), with the textured rate being typically the highest similar to the aforementioned Std-OIT observations.

The initial HP-OIT values were similar in the textured and smooth edge, suggesting a similar distribution of antioxidants detected by HP-OIT across the thickness of the two parts of the roll. Although the difference between textured and smooth edges in residual value and depletion rate was relatively small at high temperatures (75 and 85° C), their distinction at lower temperatures (i.e., 40 and 55° C) was notable (Fig. 4; Table 2). For instance, the depletion rates for textured and smooth edges at 55° C were 0.22 and 0.44 $month^{-1}$, while the residual HP-OIT values were 348 and 630 min for *MxTA15* and *MxTsA15*, respectively. While the initial HP-OIT value of the smooth edge *MxTsA15* (1580 ± 90) was 1.6-fold higher than the initial HP-OIT of the smooth equivalent *MxF15* (990 ± 140) (Table 1), the observed depletion rates of *MxF15* were the same as *MxTsA15* at all incubation temperatures except at 55 °C (Fig. 5; Table 2). The lower HP-OIT residual values observed at

Fig. 2. Variation of the ln (normalized standard oxidative induction time (Std-OIT) (OIT_t/OIT_0)) with immersion time for the textured geomembrane and its smooth edge (*MxTA15* and *MxTsA15*) incubated in municipal solid waste leachate 3: (*a*) 55 and 85 °C and (*b*) 40 and 75 °C. Error bars represent the range of results.

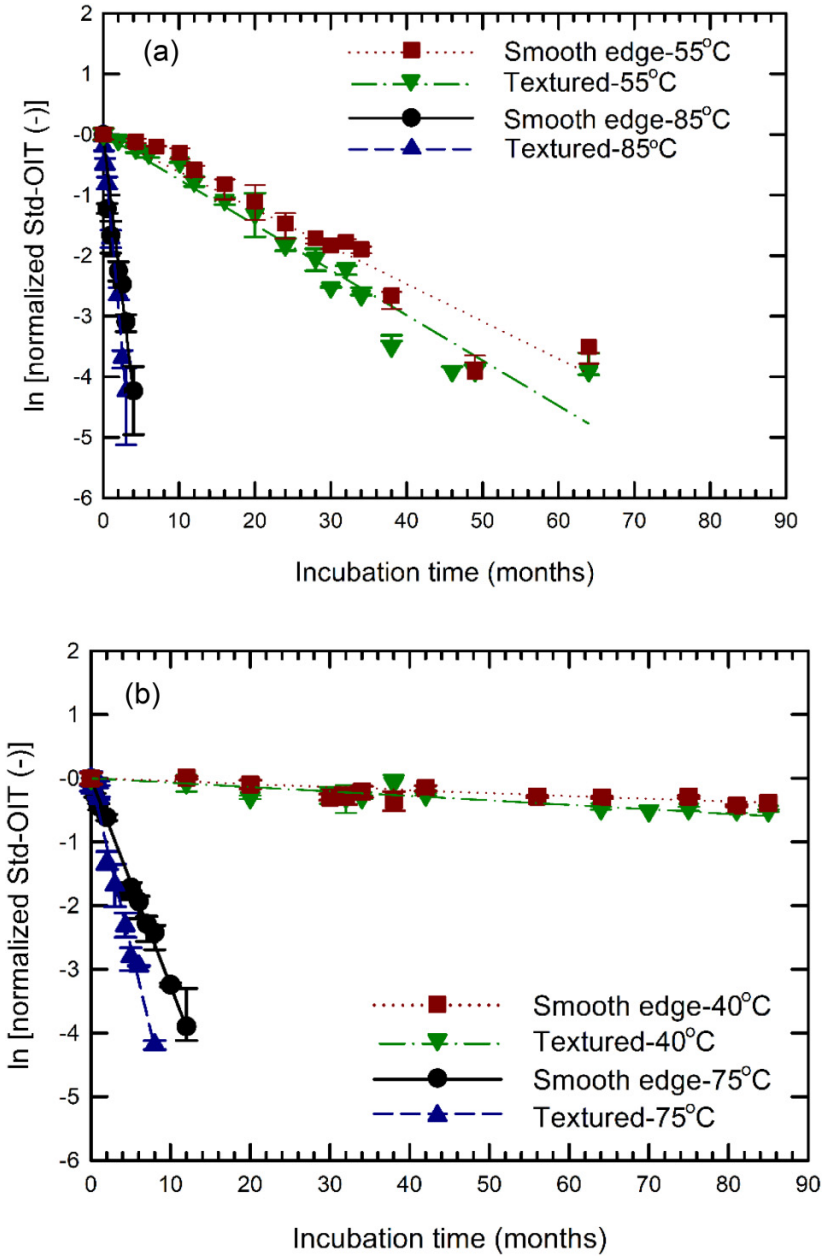

higher temperatures were probably attributed to the higher mobility of the HALS and the relative ease of outward diffusion from the GMB's core at higher temperatures (Rowe and Ewais 2014; Morsy and Rowe 2020*a*).

At higher temperatures, the variation in depletion rates between the two portions of the textured GMB was smaller based on HP-OIT compared to Std-OIT. This difference can be attributed to the lower effect of surface area and core thickness on the depletion of high molecular weight HALS (Ewais et al. 2014; Morsy and Rowe 2020*a*; Scheirs et al. 2020) than the phenolic antioxidants detected by the Std-OIT test. Nevertheless, for $T \leq 65$ °C, HP-OIT depleted to residual values faster than the Std-OIT in all cases examined here. Thus, as often is the case, the Std-OIT depletion controlled the length of Stage I of the three stages of GMB service life for $T \leq 65$ °C.

3.1.3. Antioxidant depletion stage prediction

3.1.3.1. Basics

Arrhenius modelling (Arrhenius 1889*a*, 1889*b*; Koerner et al. 1992) was used to predict the rate of antioxidant depletion at lower temperatures, using the depletion rates obtained experimentally for Std-OIT and HP-OIT. The Arrhenius equation can be written as

$$s = Ae^{-(E_a/RT)} \quad (4)$$

Table 2. Observed OIT depletion rates and residual values.

Temperature (°C)	GMB	*MxTA15*	*MxTsA15*	*MxF15*
40	$S_{std\text{-}OIT}$ (month^{-1})	0.007	0.0051	0.0063
	Std-OIT$_r$ (min)	N/A[a]	N/A[a]	N/A[a]
	$S_{HP\text{-}OIT}$ (month^{-1})	0.014	0.013	0.009
	HP-OIT$_r$ (min)	N/A[b]	N/A[b]	N/A[b]
55	$S_{std\text{-}OIT}$ (month^{-1})	0.076	0.065	0.065
	Std-OIT$_r$ (min)	4	4	3
	$S_{HP\text{-}OIT}$ (month^{-1})	0.036	0.037	0.034
	t_d (months)	54	64	60
	HP-OIT$_r$ (min)	348	630	238
75	$S_{std\text{-}OIT}$ (month^{-1})	0.53	0.33	0.48
	Std-OIT$_r$ (min)	3	4	3
	t_d (months)	8	12	8
	$S_{HP\text{-}OIT}$ (month^{-1})	0.095	0.08	0.085
	HP-OIT$_r$ (min)	220	220	198
85	$S_{std\text{-}OIT}$ (month^{-1})	1.42	1.07	1.51
	Std-OIT$_r$ (min)	3	3	2
	t_d (months)	3	4	3
	$S_{HP\text{-}OIT}$ (month^{-1})	0.389	0.304	0.251
	HP-OIT$_r$ (min)	220	220	198

Note: GMB, geomembrane; HP-OIT, high-pressure oxidative induction time; Std-OIT, standard oxidative induction time.
[a]The Std-OIT has not depleted to a residual value yet. [b]The HP-OIT has not depleted to a residual value yet.

where s (month^{-1}) is the depletion rate, A (month^{-1}) is the collision factor, E_a (J.mol^{-1}) is the activation energy for antioxidant depletion, R (J/mol^{-1}.K^{-1}) is the universal gas constant equals 8.314 J/(mol.K), and T (K) is the absolute temperature. Taking the natural logarithm on both sides of eq. 4 gives

$$\ln(s) = \ln(A) - \left(\frac{E_a}{R}\right)\left(\frac{1}{T}\right) \quad (5)$$

For the Std-OIT depletion, the parameters E_a and A were estimated by plotting the natural logarithm of depletion rates against the inverse of the absolute temperatures for all incubated temperatures (Figs. 6*a* and 7*a*). Based on 8 years of aging using an average depleted Std-OIT$_d$ value of 3 min, the Std-OIT depletion times for *MxTA15*, *MxTsA15*, and *MxF15* were predicted and compared with and found to be in encouraging agreement with observed values (Table 3). Predictions were then made at temperatures between 10 and 85 °C based on the best-fit data at 85, 75, 55, and 40 °C and Arrhenius plots such as that shown in Figs. 6 and 7 and the corresponding predictions are given in Table 4.

3.1.3.2. *Effect of texturing on Std-OIT depletion immersed in MSW L3 at typical landfill temperatures*

Based on a typical MSW landfill temperature of about 40 °C, the expected values given in Table 4, the Std-OIT of the smooth edge would take 30% longer to deplete than the textured portion. Thus, the use of a textured GMB where it is not needed (most of the base of most landfills) notably compromises the potential service life compared to the "equivalent" smooth roll. The practical implications of this will be explored again later.

3.1.3.3. *Uncertainty in predictions of time to Std-OIT depletion*

Inspection of Figs. 6 and 7 shows that the 55 °C data depart somewhat for the best fit to the four data points. When comparing the predicted and observed depletion times at 85, 75, and 55 °C (40 °C still has not fully depleted), the agreement is good for 75 and 85 °C and not so good for the expected value at 55 °C. This raises the question of uncertainty in predictions. This question can be addressed by constructing the 95% confidence limits on the data and this results in three predictions: (i) the expected depletion time (and depletion rate) based on the "best fit" predictions (50% probability of the depletion time will be above, and a 50% probability will be below, this value); (ii) a minimum prediction with a 95% probability of being exceeded; and (iii) a maximum prediction with a 95% probability that the actual depletion time will be less than this value. Values for time to OIT depletion and the rates were obtained from the curves in Figs. 6 and 7 for all three GMBs (*MxTA15*, *MxTsA15*, and *MxF15*) as indicated in the supplementary material (Tables S1 and S2). The minimum and expected values of time to OIT depletion are given in Table 5.

The Std-OIT data for the textured portion shown in Fig. 8 (black circles) contain notable scatter. Based on the Arrhenius modelling, the expected depletion rate ($s = 0.059$ mo^{-1}) shown as the blue dot–dash line provides a good general description of the data, with values on either side of the curve, and it particularly well captures the last data point. This curve corresponds to a depletion time of 70 months (5.9 years). The brown long-dashed curve ($s = 0.076$ mo^{-1}) corresponds to the minimum depletion time of 54 months (4.5 years) and also corresponds to the best fit to the data overall. The red short-dashed curve ($s = 0.045$ mo^{-1}) provides the best description

Fig. 3. Variation of the ln {normalized Std-OIT (OIT_t/OIT_0)} with immersion time for the smooth edge and its equivalent smooth geomembrane (*MxTsA15* and *MxF15*) incubated in municipal solid waste leachate 3: (*a*) 40 and 75 °C and (*b*) 55 and 85 °C. Error bars represent the range of results. Std-OIT, standard oxidative induction time.

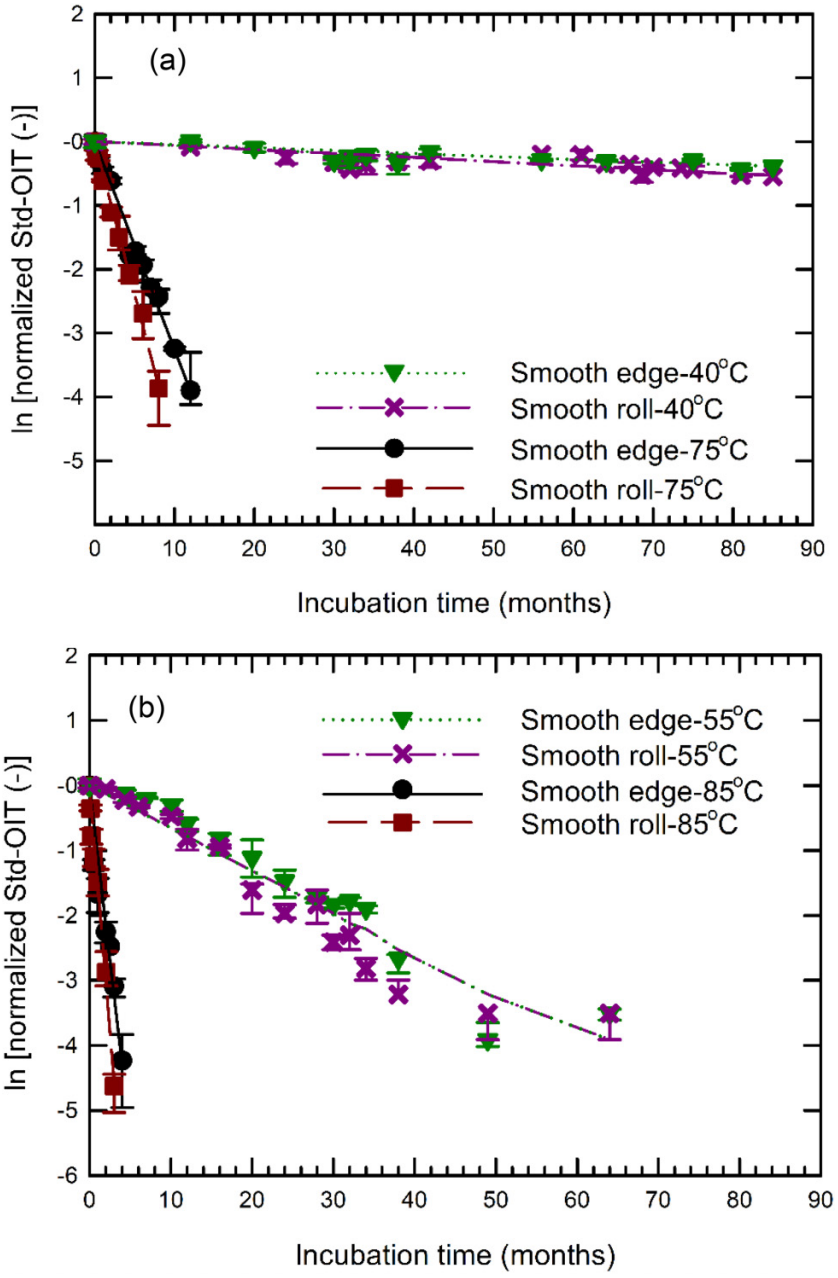

of the early time data and corresponds to the maximum time to depletion of 92 months (7.6 years). Since it represents the 95th percentile, essentially all data points are either on or below this curve.

The antioxidants have not been depleted at 40 °C, but the predicted depletion rates can be compared with the observed data (Fig. 9). The green dot–dot–dashed curve ($s = 0.021$ mo^{-1}) for the minimum time to depletion (16.9 years) has all of the data points above it and is seen to be quite conservative. The blue dot–dashed curve ($s = 0.009$ mo^{-1}) for the expected time to depletion captures the scatter of the early time data but overpredicts the depletion at later times, and its corresponding depletion time of 38 years is likely very conservative (i.e., it underestimates the time to OIT depletion). Based on the first author's experience and judgement, the brown long-dashed curve ($s = 0.007$ mo^{-1}) is considered the "best fit" and corresponds to a depletion time of 49 years. The red short-dashed curve ($s = 0.0039$ mo^{-1}) for the maximum time to depletion of 88 years has all data either on or below it.

Similar curves were established for *MxTA15*, *MxTsA15*, and *MxF15* times to a minimum and expected depletion, as given in Tables 5 and 6. In all cases, the observed time to depletion fell within the predicted range (Table 3).

Fig. 4. Variation of the normalized high-pressure oxidative induction time (HP-OIT) (OIT_t/OIT_0) with incubation time for the smooth edge of the textured geomembrane (GMB) and textured GMB (*MxTsA15* and *MxTA15*) immersed in municipal solid waste leachate 3: (*a*) 40 and 75 °C and (*b*) 55 and 85 °C. Error bars represent the range of results.

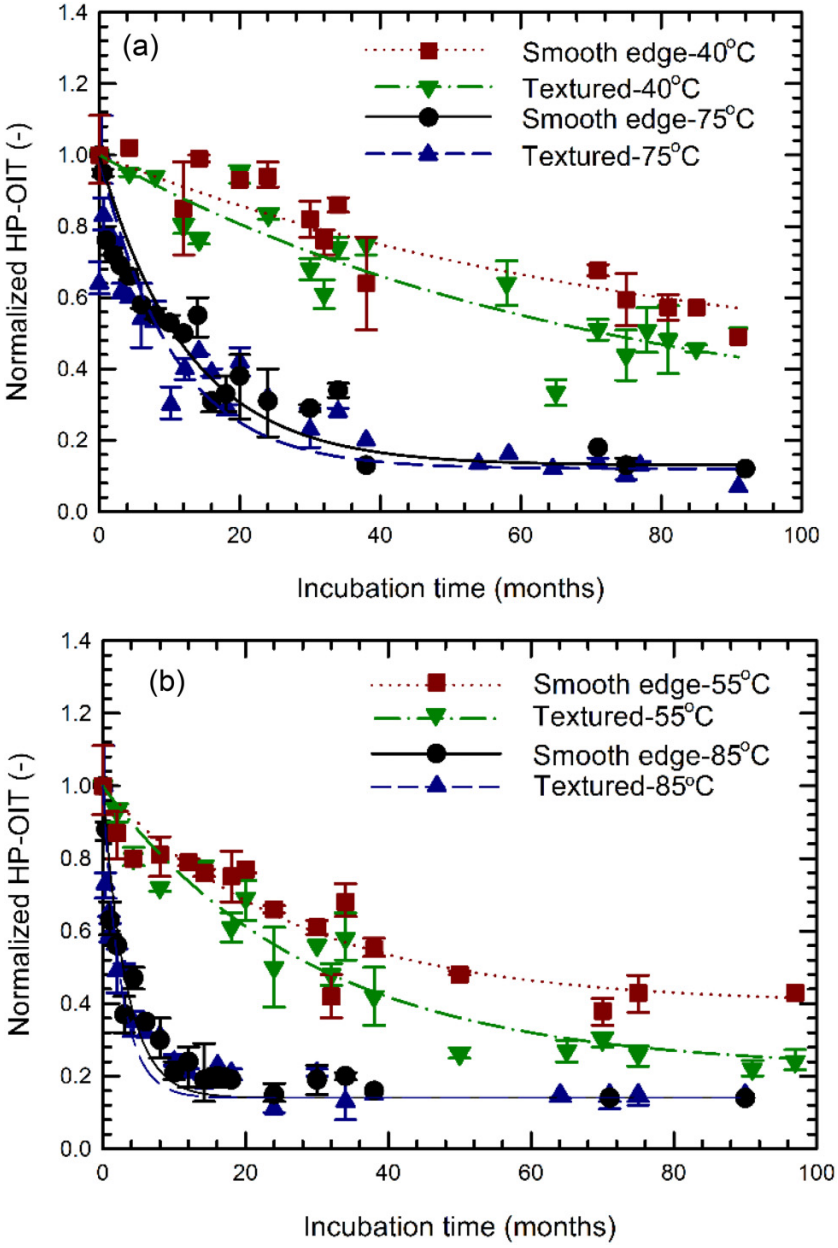

3.1.3.4. Comparison with the Morsy and Rowe (2020a)

The expected times to Std-OIT depletion from the 34 months of testing in the Morsy and Rowe (2020*a*) study can be compared with a total of 94 months of data, as summarized in Table 7. The predictions for both the textured (*MxTA15*) and smooth edge (*MxTsA15*) portions show an excellent agreement with the Morsy and Rowe (2020*a*) values, which are slightly conservative (i.e., erring on the low side). However, the same is not true for the smooth equivalent (*MxF15*). For this GMB, the Morsy and Rowe (2020*a*) predictions were notably lower (more conservative) than those obtained in the current study. The difference can be explained by inspecting Fig. 10 and noting the data that were available over the first 34 months resulted in black solid best-fit curve ($s = 0.011$ mo^{-1}), while the brown long-dashed curve, representing the best fit to the full dataset available for this paper, has almost half the slope ($s = 0.0063$ mo^{-1}) with the correspondingly longer times to depletion that is now apparent. Thus, it can be concluded that 34 months were adequate for predicting depletion times with well-behaved data at the lowest temperature of 40° C, but with uncertain data as in the case for *MxF15*, more immersion time was required. The anomalous data used in the predictions by Morsy and Rowe (2020*a*) have not been excluded and consequently the uncertainty reflected by the difference between the green dot–dot–dashed maximum and red short-dashed minimum prediction curves. The change in behaviour

Fig. 5. Variation of the normalized high-pressure oxidative induction time (HP-OIT) (OIT_t/OIT_0) with incubation time for the smooth edge and equivalent smooth (*MxTsA15* and *MxF15*) immersed in municipal solid waste leachate 3: (*a*) 40 and 75 °C and (*b*) 55 and 85 °C. Error bars represent the range of results.

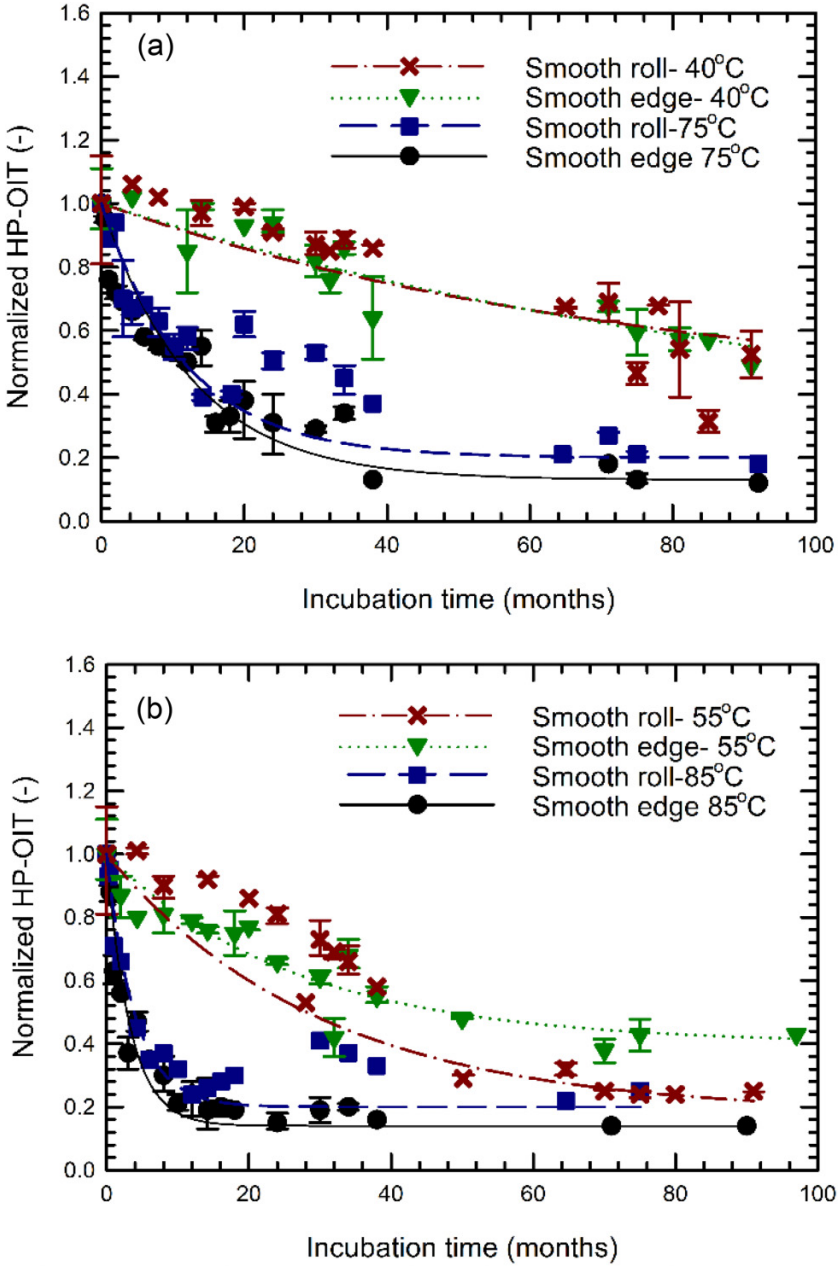

between about 30 and 45 months was likely a reflection of the final depletion of one component of the antioxidant package, as detected by the Std-OIT test, with the remaining component exhibiting a much slower depletion rate that was initially masked by the faster depletion of the originally more dominant component of the antioxidant package.

3.1.3.5. HP-OIT depletion

The HP-OIT depletion rates, *s*, obtained at temperatures ranging from 40 to 85 °C in MSW-L3 (Table 2), were utilized to establish the Arrhenius plot (Figs. 4 and 5) for extrapolating antioxidant depletion rates at lower temperatures. Both the depletion rate and residual HP-OIT values ($HP\text{-}OIT_r$) are required to be substituted into eq. 5. The results (Figs. 4*b* and 5*b*) show no clear pattern in the variation of $HP\text{-}OIT_r$ with decreasing temperature. The observed differences in $HP\text{-}OIT_r$ at most temperatures showed no statistically significant difference, consistent with other studies (e.g., Clinton and Rowe 2023 and Abdelaal et al. 2019). This may be attributed to the inter-related properties (i.e., polymer free-volume and stabilizer solubility), which are both temperature-dependent properties (Clinton and Rowe 2023). Thus, the residual value was estimated as the average observed $HP\text{-}OIT_r$ at higher temperatures (i.e., Figs. 4 and 5). These values were used to predict the HP-OIT depletion times at different temperatures. At tem-

Fig. 6. Arrhenius plot of OIT depletion for the textured geomembrane (GMB) and its smooth edge (*MxTA15* and *MxTsA15*): (*a*) standard oxidative induction time (Std-OIT) and (*b*) high-pressure oxidative induction time (HP-OIT).

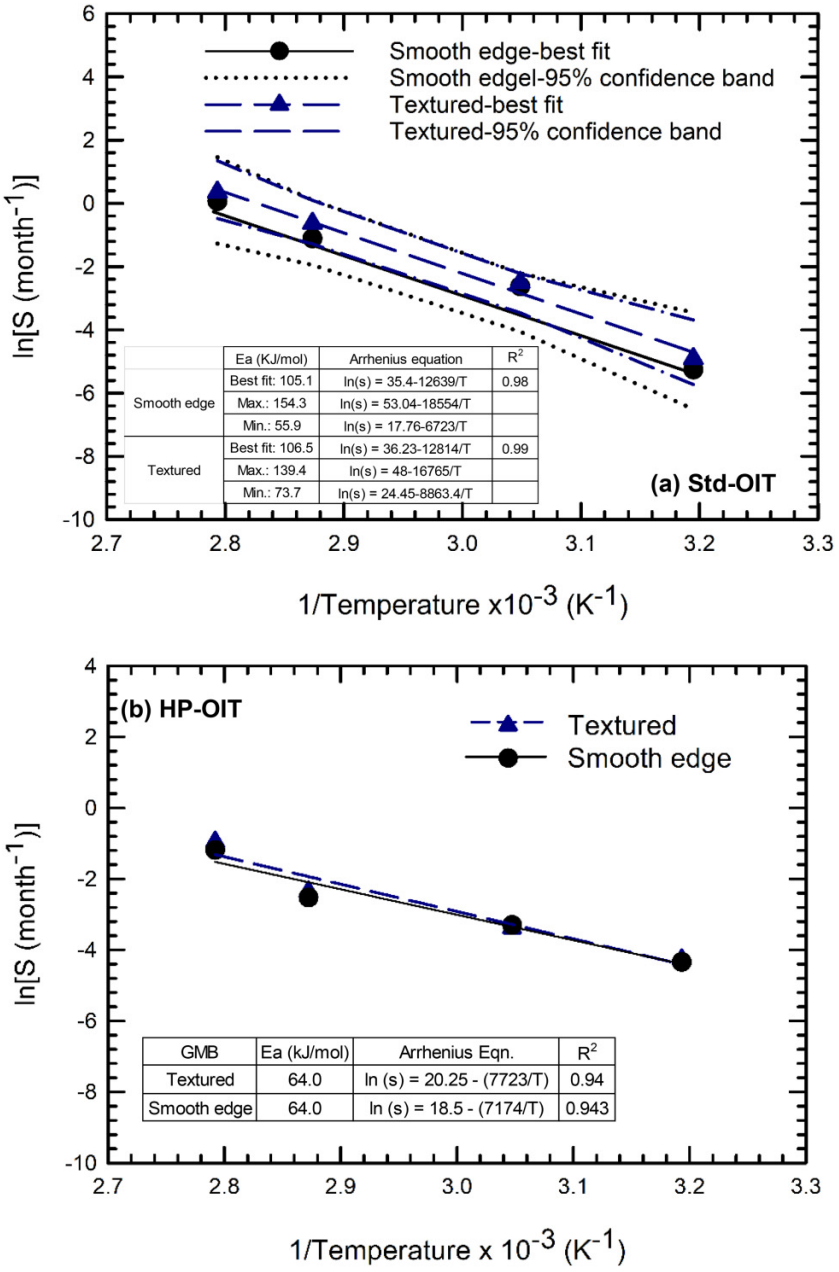

peratures > 65 °C, the HP-OIT depletion time was longer than those observed using Std-OIT (Table 3). Using the Arrhenius equations in Figs. 6*b* and 7*b* to extrapolate the HP-OIT depletion time at 40 °C (to the residual value), gave predictions of 13.5, 13.5, and 14.3 years for *MxTA15*, *MxTsA15*, and *MxF15*, respectively. Hence, the small difference in depletion rates and residual values between the textured and smooth-edge portion of the GMBs was observed at higher temperatures, and a negligible impact on the time to HP-OIT depletion of the GMBs was observed at lower field temperatures.

An examination of Tables 3 and 4 reveals that the predicted antioxidant depletion times based on HP-OIT at temperatures < 65 °C were shorter than those predicted based on Std-OIT depletion. For instance, at 40° C, the predicted HP-OIT depletion times (13.5, 13.5, and 14.3 years) of *MxTA15*, *MxTsA15*, and *MxF15* were 2.8, 3.7, and 2.9 times shorter than the corresponding Std-OIT depletion times (38, 50, and 41 years). This suggests that the Std-OIT package played a crucial role in protecting the GMB compared to the HP-OIT package within the temperature range of the GMB liner in most geoenvironmental applications (T < 65 °C).

3.2. Melt flow index

The variation of the normalized HLMI of the three GMBs was monitored at all temperatures (40, 55, 75, and 85 °C). It showed no changes during the 98 months of incubation at lower temperatures (i.e., 40 and 55 °C), but there was

Fig. 7. Arrhenius plot of OIT depletion for the textured geomembrane (GMB) and its smooth edge (*MxTA15* and *MxTsA15*): (*a*) standard oxidative induction time (Std-OIT) and (*b*) high-pressure oxidative induction time (HP-OIT).

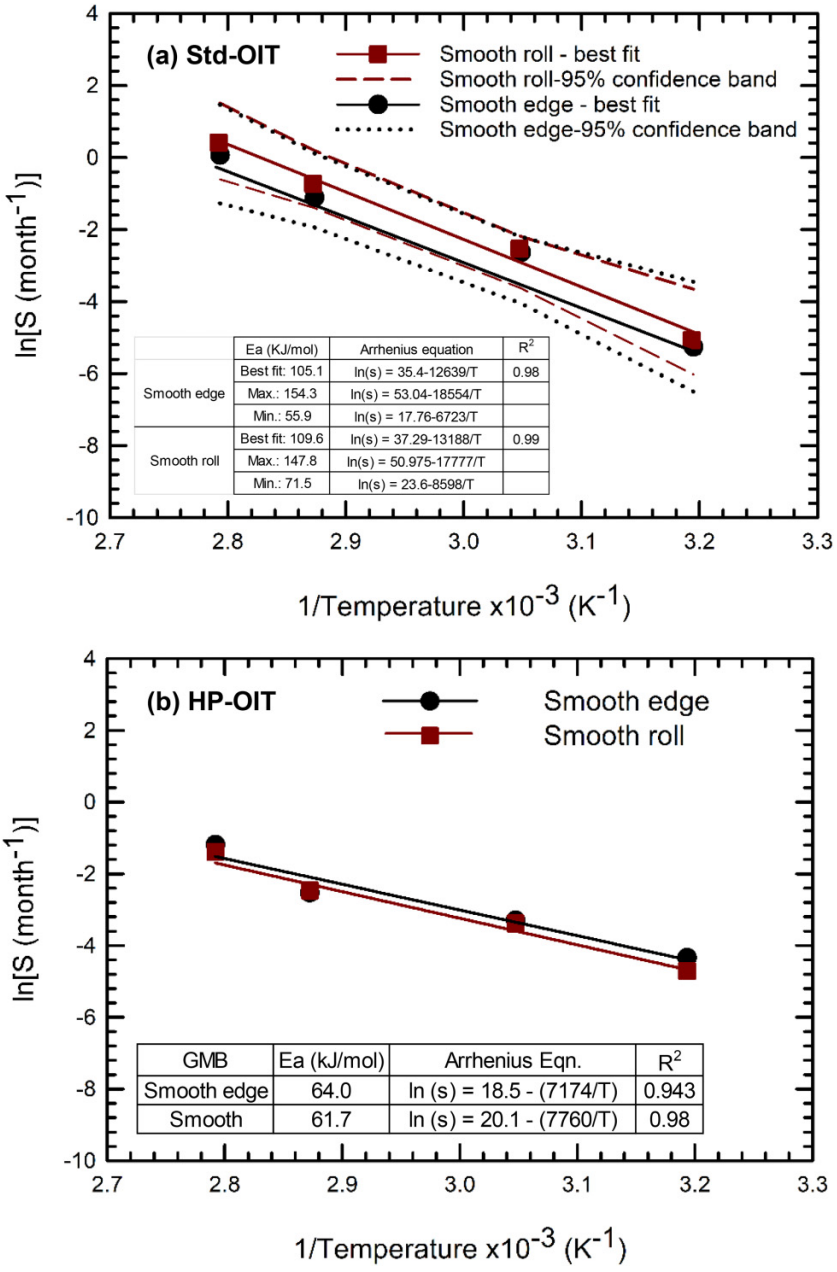

	Ea (KJ/mol)	Arrhenius equation	R^2
Smooth edge	Best fit: 105.1	ln(s) = 35.4-12639/T	0.98
	Max.: 154.3	ln(s) = 53.04-18554/T	
	Min.: 55.9	ln(s) = 17.76-6723/T	
Smooth roll	Best fit: 109.6	ln(s) = 37.29-13188/T	0.99
	Max.: 147.8	ln(s) = 50.975-17777/T	
	Min.: 71.5	ln(s) = 23.6-8598/T	

GMB	Ea (kJ/mol)	Arrhenius Eqn.	R^2
Smooth edge	64.0	ln (s) = 18.5 - (7174/T)	0.943
Smooth	61.7	ln (s) = 20.1 - (7760/T)	0.98

a change for the 75 °C (Fig. S1) and 85 °C (Figs. 11 and 12). At 85 °C, the HLMI remained unchanged during the first 20 months of immersion and then started decreasing, implying dominant cross-linking oxidation reactions (Figs. 11 and 12). After 40 months of incubation, the HLMI of all examined GMBs (*MxF15*, *MxTsA15*, and *MxTA15*) had decreased to 50% of their initial value at 85 °C. The similar degradation trends of the textured GMB and its smooth edge suggest that texturing had a negligible effect on the molecular weight distribution during the degradation of the GMB.

Despite the smooth edge and smooth "equivalent" manufactured from the same resin but different resin lots, both GMBs exhibited different initial HLMI values. However, their HLMI behaviour was similar, and both had reduced to 50% of the initial value after 40 months of incubation.

The reduction in HLMI value at 75 °C observed after 85 months lies within the range of variability observed over the aging time, and there is uncertainty as to whether it is really decreasing or the results are just scattered—time will tell.

3.3. Tensile properties

An additional 64 months of data were added to the 34 months of incubation data reported by Morsy and Rowe (2020*a*). As aging progressed, the tensile break properties of the textured GMB exhibited variability around the best-fit

Fig. 8. Variation in standard oxidative induction time (Std-OIT) with incubation time and various predictions for the textured portion (*MxTA15*) at 55 °C: (*a*) Std-OIT versus incubation time and (*b*) (ln(Std-OIT) − ln(std OITo)) versus incubation time.

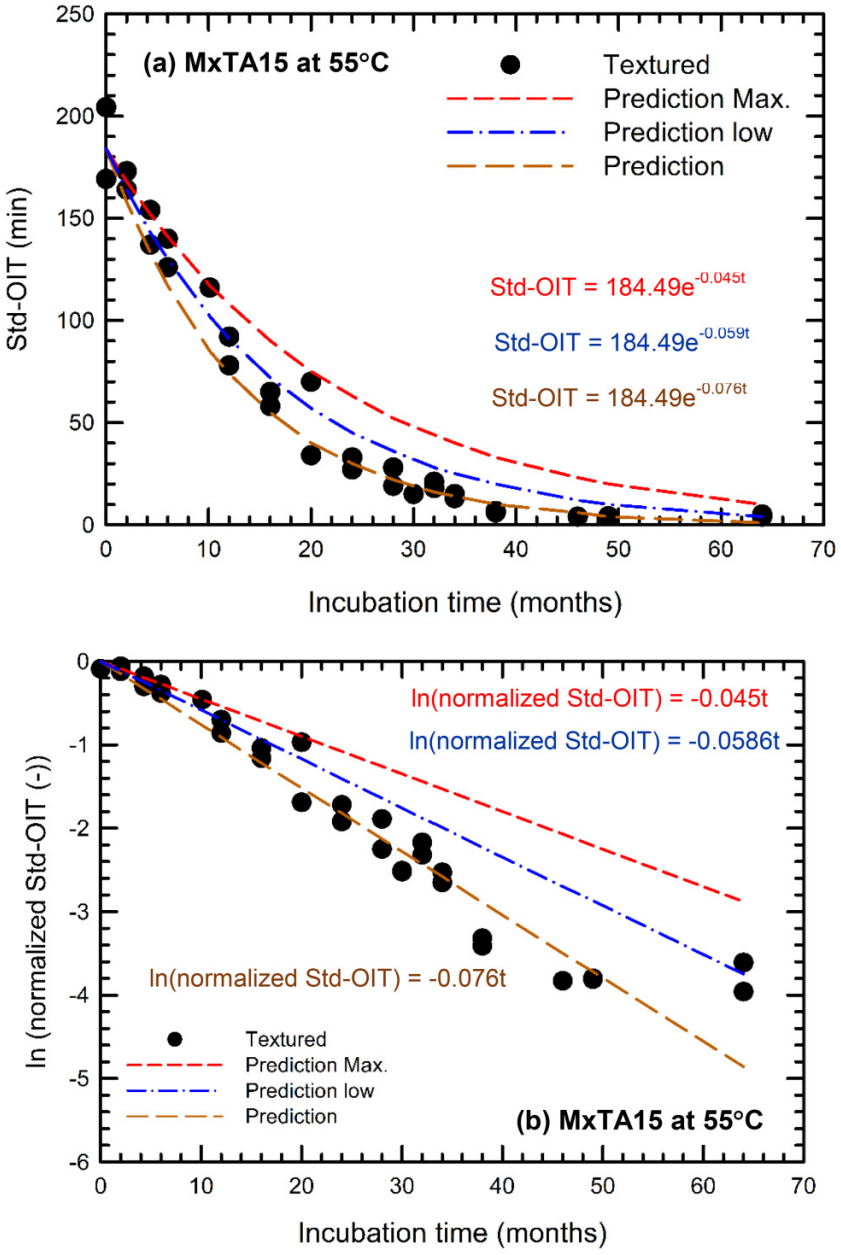

line at all temperatures. At 85 °C, all GMBs showed a reduction in the break properties. The break strain of *MxTA15*, *MxTsA15*, and *MxF15* started to decrease after 34 months, reaching 50% of the initial values (t_{NF} at 60, 80, and 80 months, respectively; Figs. 13*a* and 13*b*). Similarly, all GMBs retained their break strength during the first 34 months and then started to decrease, reaching 50% after 60 months at 85 °C (Figs. 13*c* and 13*d*).

As with the HLMI results, the degradation behaviour of tensile break properties was similar for smooth and smooth-edge GMBs. While the tensile properties showed longer retention times than the HLMI for all GMBs, polymer degradation based on tensile break properties was detected in *MxTA15* faster than *MxTsA15* and *MxF15*. Texturing increases the surface area of the GMB exposed to leachate compared to the smooth edge and allows the salts to precipitate with higher concentration at the grooves between the asperities. The mechanisms other than diffusion affecting depletion of antioxidants and subsequent degradation in MSW-L3 are uncertain. What is clear, however, is that texturing the surface increases the susceptibility of faster degradation and notable variation in break strength (Morsy and Rowe 2020*a*). The substantial variability in break strain suggests that the t_{NF} may occur in less than 64 months. For instance, the normalized break strain after 50 months of incubation exhibits considerable variability, with values ranging from a low of 0.12 to a high of 0.9 (Fig. 13*a*). However, the break strength and elongation are not critical for a GMB since the strain level in the field should be below

Fig. 9. Variation in (ln(Std-OIT)-ln(std OITo)) versus incubation time and various predictions for the textured portion (*MxTA15*) at 40 °C. Std-OIT, standard oxidative induction time.

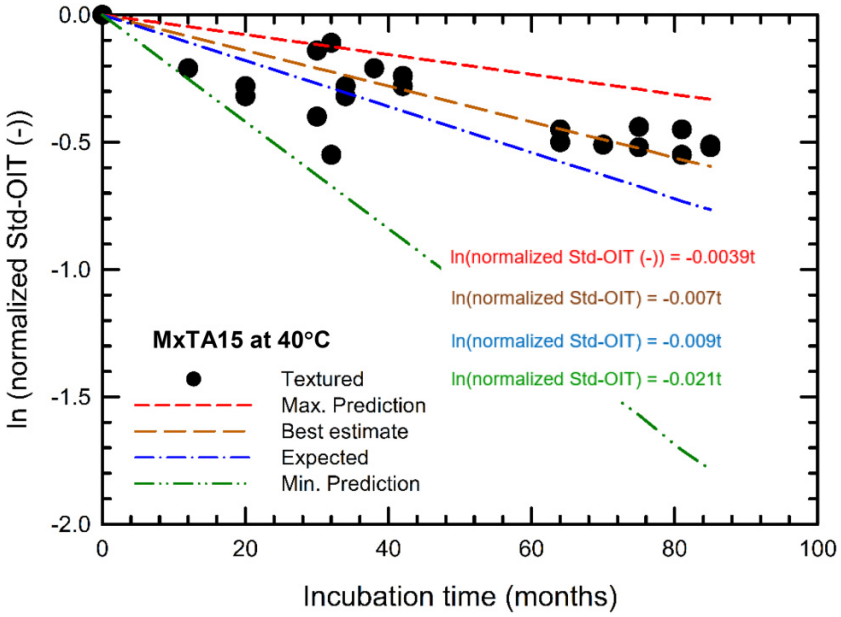

Table 3. Observed and predicted times (years) to OIT depletion and nominal failure immersed in municipal solid waste leachate 3.

		$t_{d\ Std\text{-}OIT}$ (years)		$t_{d\ HP\text{-}OIT}$ (years)		$t_{NF\ SCR}$ (years)		$t_{NF\ HLMI}$ (years)	$t_{NF\ TBS}$ (years)	$t_{NF\ TBE}$ (years)
GMB	T (°C)	Predicted[a]	Observed	Predicted[b]	Observed	Predicted[c]	Observed	Observed	Observed	Observed
MxTA15	85	0.22	0.23	0.6	0.8	2.3	2.3	3.3	5.0	5.0
MxTsA15	85	0.31	0.33	0.8	0.8	2.2	2.2	3.3	5.0	6.7
MxF15	85	0.21	0.23	0.7	1.0	1.9	1.9	3.3	5.0	6.7
MxTA15	75	0.62	0.7	1.1	3.0	6.0	6.0	–	–	–
MxTsA15	75	0.86	0.83	1.3	3.0	6.0	6.0	–	–	–
MxF15	75	0.61	0.7	1.3	3.0	6.0	6.0	–	–	–
MxTA15	55	4.5–6.1–7.6	4.5	4.4	4.2	–	–	–	–	–
MxTsA15	55	5.3–7.9–11.7	5.3	4.7	4.2	–	–	–	–	–
MxF15	55	4.5–6.1–8.2	5.0	4.8	4.2	–	–	–	–	–

Note: Numbers are rounded to two significant figures. GMB, geomembrane; Std-OIT, standard oxidative induction time; HP-OIT, high-pressure oxidative induction time; SCR, stress crack resistance; HLMI, high-load melt index.
[a]Predicted Std-OIT depletion time based on Std-OIT residual value of 3.0 min. [b]Predicted HP-OIT depletion time based on a variable HP-OIT residual value. [c]Predicted based on $0.5SCR_m$ and only two data points at 75 and 85 °C.

the yield strain of the GMB for a well-designed barrier system. It may be hypothesized that the textured GMBs with a different structure to the texturing that are manufactured by flat die extrusion may behave differently to GMBs with the texturing arising from a blown-film texturing process. In particular, it may be hypothesized that the issue with the structured texturing will be faster depletion of the antioxidants for the stubs providing the frictional resistance and stress cracking at the root of those scrubs causing a loss in frictional capacity over time prior to failure of the sheet itself. However, no study has yet examined this hypothesis, and further investigation is needed.

No degradation in tensile break strain and strength values was observed at 98 months of incubation at 75 °C (Figs. S2 and 3), even though the SCR was fully degraded.

3.4. SCR

According to Abdelaal et al. (2024), the stress applied to the single-notch textured specimens is separated into two components: uniaxial tensile stress and bending stress caused by the offset between the centerline of the unnotched thickness of the specimens and the neutral axis of the ligament (Fig. 14). Thus, the variability in the notch depth in textured GMB (resulted from the textured surface) may affect the SCR values and result in variability of the SCR. The sources of variability of SCR of the GMBs examined in the current study were investigated by Morsy and Rowe (2020*b*) by comparing the SCR obtained from the NCTL and the crack propagation rate predicted using the principles of fracture mechanics and the fracture surfaces scanned using the environmental scanning electron microscope. The lower SCR value of the textured

Fig. 10. Variation in standard oxidative induction time (Std-OIT) with incubation time and various predictions for the smooth equivalent (*MxF15*) at 40 °C.

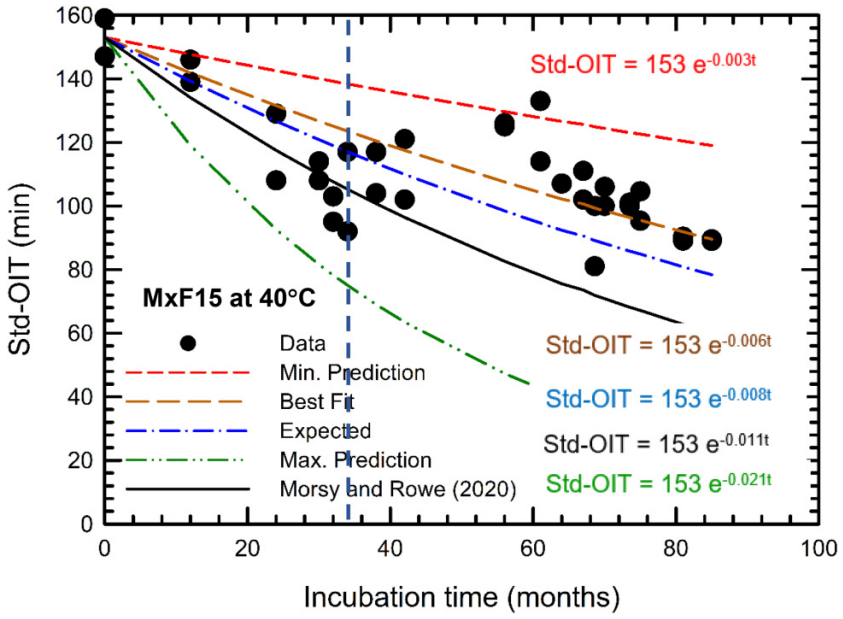

Table 4. Predicted (expected) times, t_d (years) to OIT depletion (Stage I) and length of stages II and III, ($t_{NF\_SCR} - t_{dStd\text{-}OIT}$), to nominal failure immersed in municipal solid waste leachate 3.

	$t_{d\ Std\text{-}OIT}$ (years)			$t_{d\ HP\text{-}OIT}$ (years)			($t_{NF\_SCR} - t_{d\ Std\text{-}OIT}$) (years)		
Temperature (°C)	Textured *MxTA15*	Smooth edge *MxTsA15*	Smooth roll *MxF15*	Textured *MxTA15*	Smooth edge *MxTsA15*	Smooth roll *MxF15*	Textured *MxTA15*	Smooth edge *MxTsA15*	Smooth roll *MxF15*
85	0.2	0.3	0.21	0.6	0.8	0.7	2.1	1.9	1.7
75	0.6	0.9	0.61	1.1	1.3	1.3	5.4	5.1	5.4
65	1.8	2.5	1.84	2.2	2.5	2.5	14	15	18
55	5.9	7.9	6	4.4	4.7	4.8	41	47	66
45	20	26	21	9.2	9.4	9.9	125	160	260
40	**38**	**50**	**41**	**14**	**14**	**14**	**220**	**300**	540
35	74	96	81	20	20	21	410	590	1,100
30	**150**	**190**	**160**	**31**	**29**	**31**	**760**	**1200**	**2400**
25	300	380	340	47	43	47	1,400	2,300	>5000
20	**620**	**790**	**710**	**73**	**65**	**72**	**2800**	**4800**	**>5000**
15	1300	1700	1600	110	99	110	>5000	>5000	>5000
10	2900	3600	3600	180	150	180	>5000	>5000	>5000

Note: $t_{dStd\text{-}OIT}$ and $t_{d\ HP\text{-}OIT}$ are based on data at four temperatures (40–85 °C) but ($t_{NF\_SCR} - t_{dStd\text{-}OIT}$) is only based on two temperatures (75 and 85 °C) and is far less certain.

GMB was attributed to low local SCR values related to stress concentrations at asperities, and surface defects and discontinuities at the GMB surface opposite to the notch side.

Assuming all the textured GMBs examined had the same actual thickness at the location of the notch and the applied force (F_{SCR}, i.e., 30% of F_y) was similar for various notching depths/ligament thicknesses, then for the specimens immersed at 55 and 75 °C, the SCR in Stage II (equal to the post physical aging equilibrium SCR value designated as SCR_m) decreased with an increase in the notch depth and consequent decrease in ligament thickness (Fig. 15). The SCR_m decreased by 73% with an increase in the notching depth from 0.325 (22% of the actual thickness) to 0.5 mm (33% of the actual thickness) for textured GMBs at 75° C (Fig. 15*b*). At 55 °C, the SCR_m decreased by 53% with an increase in notching depth from 0.3 (20% of the actual thickness) to 0.5 mm (33% of the actual thickness) for textured GMBs. This is attributed to the bending stress resulting from the eccentricity arising from the increase in notching depth (Fig. 14).

The maximum stresses (σ_{max}) on the specimens were calculated using eq. 6, proposed by Abdelaal et al. (2023*b*),

$$\sigma_{max} = \frac{3 \times t_N + t_L}{b.t_L^2} F_{SCR} \quad (6)$$

where F_{SCR} is the force applied to the SCR specimen, t_L is the ligament thickness of the SCR specimen, t_N is the notched depth of the specimen, b (mm) is the width of the thin part

Fig. 11. Variation of normalized high-load melt flow index (MI_t/MI_0) with incubation time for the textured geomembrane and its smooth edge (*MxTA15* and *MxTsA15*) immersed in municipal solid waste leachate 3 at 85 °C. Error bars represent the range of results. HLMI, high-load melt index.

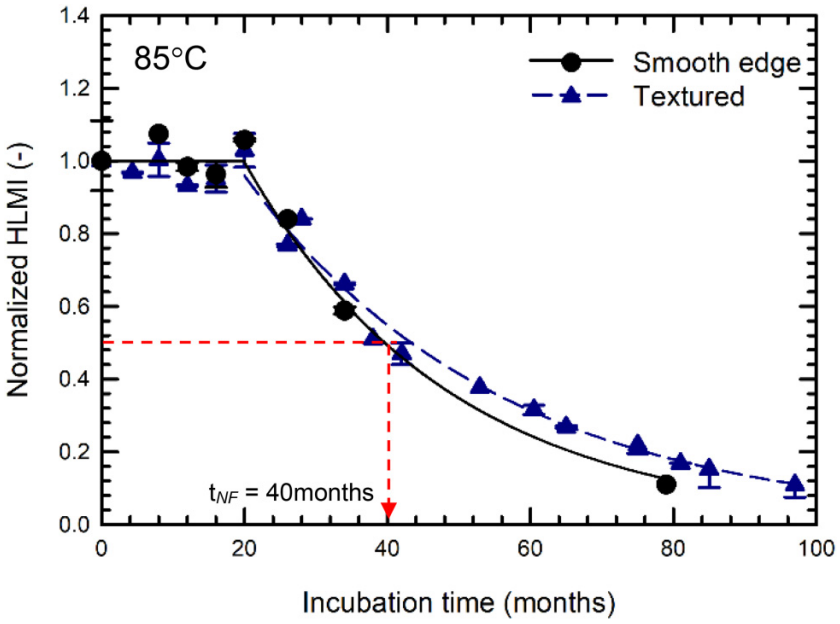

Fig. 12. Variation of normalized high-load melt flow index (MI_t/MI_0) with incubation time for the smooth edge of textured geomembrane (GMB) and its equivalent smooth GMB (*MxTsA15* and *MxF15*) immersed in municipal solid waste leachate 3 at 85 °C. Error bars represent the range of results. HLMI, high-load melt index.

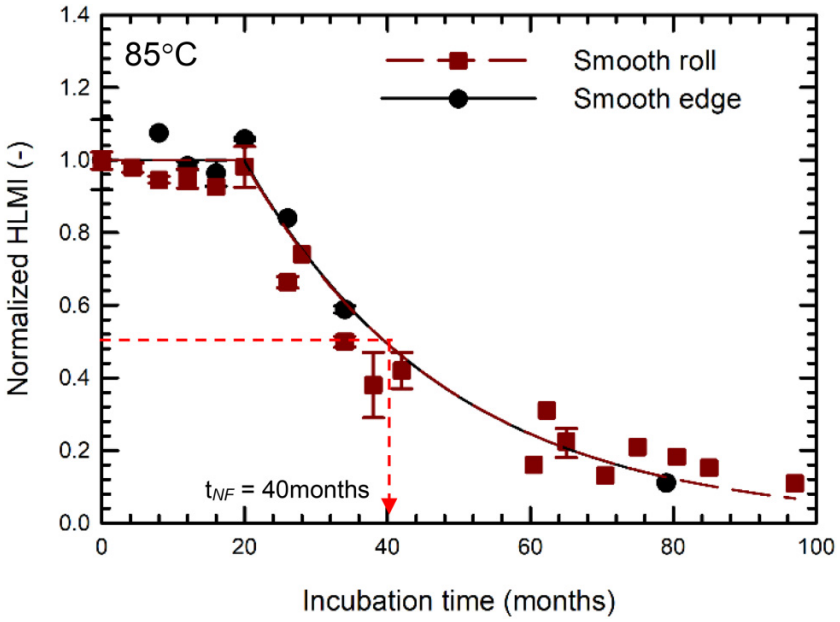

of the dog-bone specimen ($b = 3.2$ mm), and the relationship between SCR and σ_{max} is shown in Fig. 16.

For unnotched specimens and in the absence of eccentricity, the unnotched SCR of the textured GMB after 74 and 80 months incubation at 55 °C was 4600 ± 110 h at $\sigma_{max} \approx 0.67F_{SCR}/b.t$ (with only uniaxial force). Notching of these GMBs reduced SCR to 1780 h (49 mil; $\sigma_{max} \approx 1.37F_{SCR}/b.t$) and 1030 h (48 mil; $\sigma_{max} \approx 1.46F_{SCR}/b.t$) after 74 and 80 months of incubation at 55 °C, respectively (Fig. 14). This highlights the effect of notch depth on SCR variability, even when the same applied force is used. Therefore, to compare the SCR values of textured and its smooth-edge GMBs, one must consider the effect of notch depth and maintain the same t_L/t to ensure the same maximum stresses (σ_{max}) are applied to the notch tips, enabling a valid comparison between SCR values.

Fig. 13. Variation of the normalized tensile break properties—cross machine direction with incubation time for (*a*) tensile break strain for *MxTA15* and *MxTsA15*; (*b*) tensile break strain for *MxF15* and *MxTsA15*; (*c*) tensile break strength for *MxTA15* and *MxTsA15*; and (*d*) tensile break strength for *MxF15* and *MxTsA15* immersed in municipal solid waste leachate 3 at 85 °C. Error bars represent the range of results.

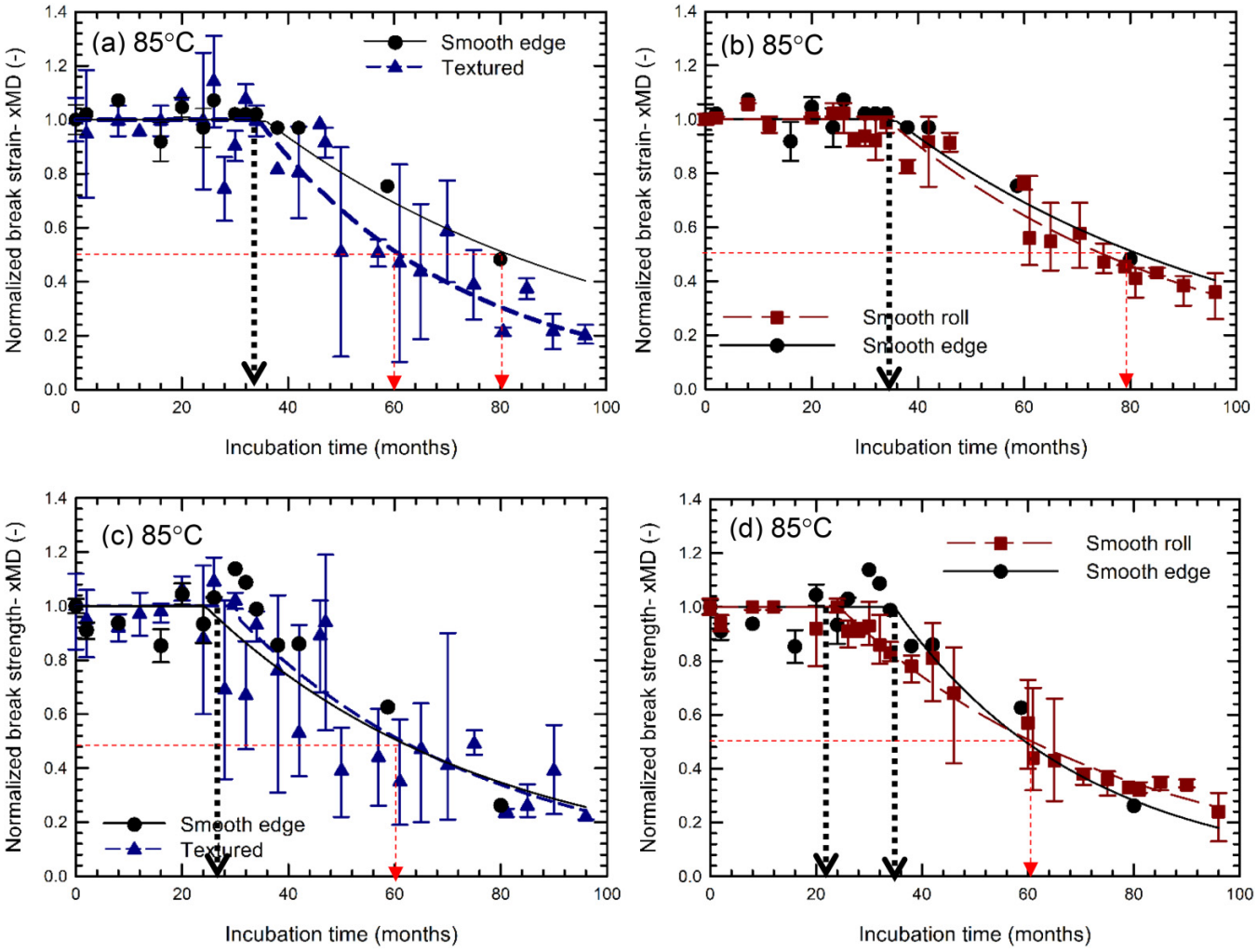

Fig. 14. Schematic diagram of the side view of single-notched stress crack resistance (SCR) specimens.

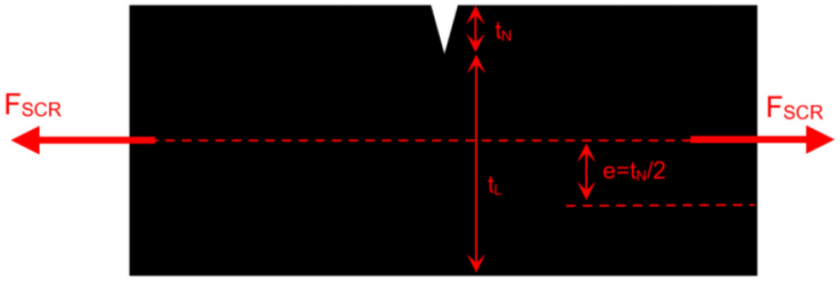

Except at 40 °C, the SCR decreased within the first 16 months of incubation from the unaged SCR_o to a stable, more representative value of SCR_m (Rowe et al. 2019; see Fig. 17). This reduction is attributed to physical aging, with no observable degradation in tensile break or MFI properties. Physical aging may occur due to morphological changes (i.e., rearrangements of the semi-crystalline structure) and/or relaxation of the manufacturing-induced residual stresses (Ewais and Rowe 2014; Rowe et al. 2019; Morsy and Rowe 2020*a*).

At 40 °C, the smooth equivalent GMB had reduced to an SCR_m 1460 ± 320 (0.38.SCR_o) h after 24 months due to the full stress relaxation. The large variability in the SCR over time of the textured GMB and its smooth edge at 40 °C may be attributed to the variation in the residual stresses on the

Fig. 15. Variation of stabilized stress crack resistance (SCR) values of textured geomembrane (*MxTA15*) with different ligament thicknesses at (*a*) 55 °C and (*b*) 75 °C.

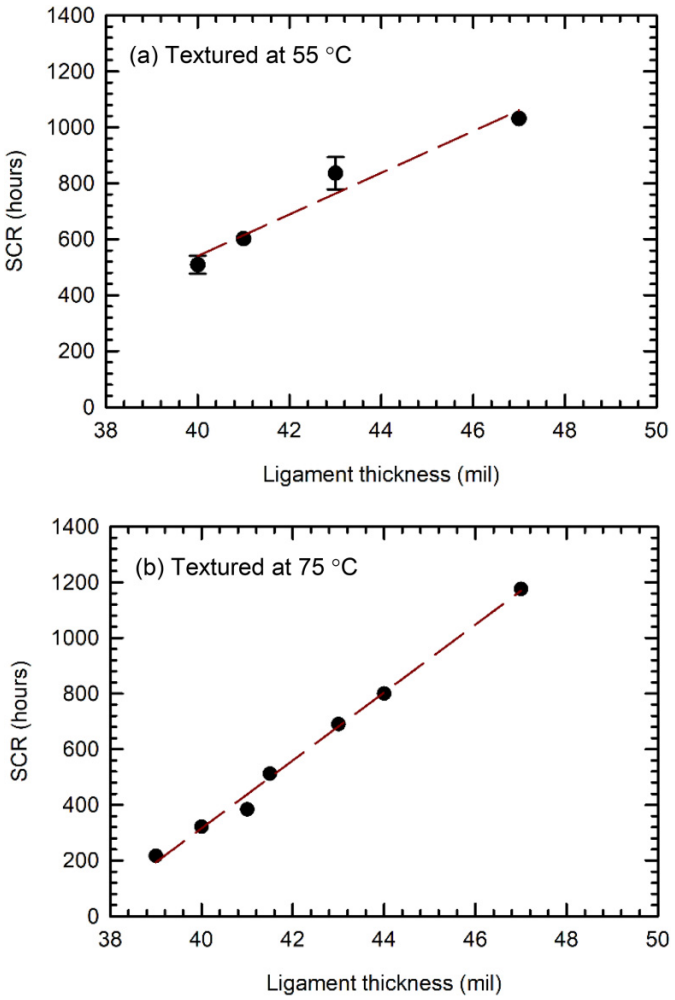

Fig. 16. Variation of stabilized stress crack resistance (SCR) values of textured (*MxTA15*) with different applied σ_{max} at the beginning of single point notched constant tensile load SCR test by changing the depth of the notch used in calculating the SCR load at (*a*) 55 °C and (*b*) 75 °C.

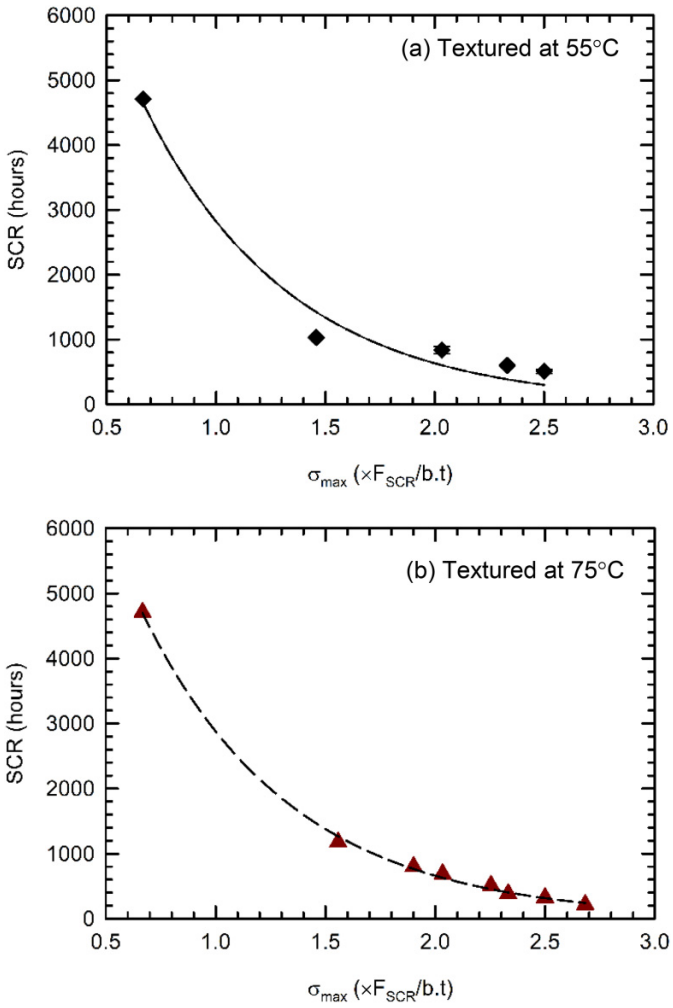

roll resulting from the nonuniform cooling during the manufacturing and the nonhomogeneity in the molten polymer flow (Chaoui et al. 1987; Xu and Bellehumeur 2008; Rowe et al. 2019) and/or variations in morphology across the roll, such as lamella thickness and the degree of short-chain branching (Ewais and Rowe 2014). This variability exists for both smooth and textured GMBs but increases for the textured GMBs due to the variability of the thickness of the sheet and/or ligament thickness of the notched sheet (strain concentration).

The average unaged SCR_o of the textured GMB was 1600 ± 1640 h (ranging from 150 to 5700 h; Morsy and Rowe 2020*a*). This calculation was based on results from specimens with a constant ligament thickness of 48 mils. SCR_m was 890 ± 340 h ($0.55.SCR_o$) for the textured portion and 1150 ± 370 h ($0.29.SCR_o$) for the smooth edge (at 55 °C); however, given the standard deviation, the difference is not statistically significant. The SCR_m of the equivalent smooth GMB was 550 ± 250 at 55 °C ($0.14.SCR_o$). The low SCR_m value is likely a result of the high residual stresses developed during the manufacturing process.

While the initial SCR_o values of the smooth equivalent GMB and the smooth edge did not show a statistically significant difference, and there are no differences in SCR_m at 75 °C or time to nominal failure (t_{NF}), a difference in SCR_m was observed at 55 °C. Similar to what was reported by Morsy and Rowe (2020*a*) at 85 °C, the SCR degradation trends at 75 °C showed the onset of chemical degradation, and t_{NF} were similar for textured and smooth edges/smooth equivalent (Figs. 17*a* and 17*b*). The degradation of SCR below SCR_m was observed in these GMBs after 24 months of immersion at 85 °C and 60 months at 75 °C in MSW-L3. With aging, the three GMBs reached t_{NF} based on 50% SCR_m after 28 months at 85 °C and 72 months at 75 °C. Based on this data and the time to Std-OIT depletion, the difference ($t_{NF\_SCR} - t_{dStd\text{-}OIT}$) can be calculated (Table 4) and using the values of $\ln(1/(t_{NF\_SCR} - t_{dStd\text{-}OIT}))$ at 75 and 85 °C to construct an Arrhenius plot, one can calculate the projected length of stages II and III as given in Table 4.

Fig. 17. Variation of the normalized stress crack resistance (SCR) (SCR_t/SCR_0) with incubation time for the textured geomembrane (GMB), its smooth edge of the textured, and equivalent smooth GMB (*MxTA15*, *MxTsA15*, and *MxF15*) immersed in municipal solid waste leachate 3: (*a*) *MxF15* and *MxTsA15* at 75 °C; (*b*) *MxTA15* and *MxTsA15* at 75 °C; (*c*) *MxF15* and *MxTsA15* at 55 °C; and (*d*) *MxTA15* and *MxTsA15* at 55 °C. Error bars represent the range of results.

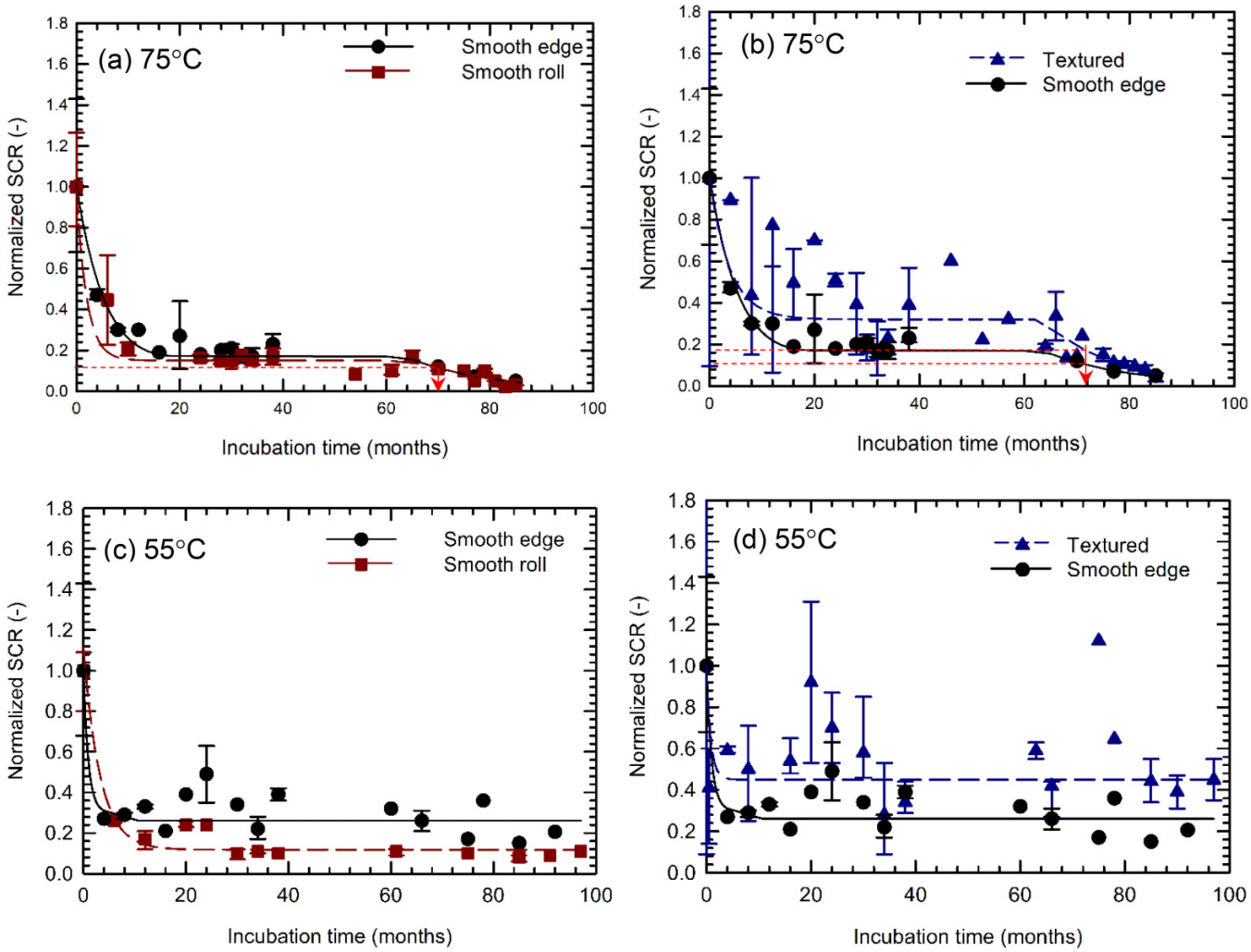

Abdelaal et al. (2014*a*) investigated the brittle failure of 1.5 mm HDPE GMBs under simulated landfill conditions using a geosynthetic liner longevity simulator. They highlighted the critical effect of a substantial decrease in SCR values of a GMB's susceptibility to brittle fractures due to gravel indentation. It was shown that GMB sheets aged to achieve a notched SCR of 75 h exhibited brittle failure, resulting in 35 000 holes per hectare at a temperature of 55 °C. This vulnerability increased with temperature, and the material was prone to brittle ruptures at strain levels as small as 6% around individual gravel indentations. In this present study, after 85 months of immersion, the textured part of the GMB showed a notched SCR value of 75 h, whereas the unnotched SCR was approximately twice as high, about 140 h. In comparison, smooth rolls made from the same type of resin exhibited a notched SCR of 75 h and an unnotched SCR of 1423 h after the same duration. This suggests that textured GMBs may become susceptible to brittle failure when exposed to strains of 6% after 85 months of incubation.

The significant difference between aged unnotched SCR (1423 h smooth and 140 h textured) and both at 75 h notched strongly suggests that the similarity in the time to nominal failure of the three GMBs based on SCR of notched specimens arises because the notch effect (stress concentration at the notch tip) dominates over the texturing effect due to the nature of the test when the SCR is degrading.

3.4.1. Effect of MSW leachate inorganic chemistry

To assess the impact of salts in the leachate on the textured GMB (*MxTA15*), textured samples were immersed in MSW-L5 (Abdelaal et al. 2014*b*). Leachate MSW-L5 has the same surfactant and trace metals as L3 but did not contain salts. Thus, comparing the performance of the same textured GMB in both leachates provides some insight into the effect of salts on GMB longevity. Thus, while *MxTA15* reached t_{NF} after 28 months at 85 °C in MSW-L3, the SCR was still 1390 ± 890 h after 90 months in MSW-L5 at 85 °C. In addition, unlike in L3,

Table 5. Predicted minimum and expected depletion standard oxidative induction time (Std-OIT) times, $t_{dStd\text{-}OIT}$ (years), length of stages II and III ($t_{NF} - t_d$), and predicted minimum and expected time to nominal failure in the field (rounded to two significant digits) $t_{NF\_Field} = 3.4 \times t_{dStd\text{-}OIT} + (t_{NF} - t_d)$.

GMB	*MxTA15*					*MxTsA15*				
Temp. (°C)	Minimum*	Expected	Stages II and III	Minimum $t_{NFfield}$	Expected $t_{NFfield}$	Minimum*	Expected	Stages II and III	Minimum $t_{NFfield}$	Expected $t_{NFfield}$
85	0.5	0.2	2.1	3.7	2.9	1.0	0.3	1.9	2.2	2.9
75	1.0	0.6	5.4	8.6	7.5	1.6	0.9	5.1	6.8	8.0
65	2.0	1.8	14	21	21	2.9	2.5	15	22.9	24
55	4.5	5.9	41	57	61	5.3	7.9	47	67.2	74
45	11	20	125	190	190	10	26	160	2.0	250
40	**16**	**38**	**220**	**280**	**360**	**14**	**50**	**300**	**360**	**470**
35	26	74	410	500	660	20	96	590	670	910
30	**42**	**150**	**760**	**900**	**1300**	**29**	**190**	**1200**	**1300**	**1800**
25	68	300	1400	1700	2500	42	380	2300	2500	3600
20	**110**	**620**	**2800**	**3200**	**4900**	**61**	**790**	**4800**	**>5000**	**>5000**
15	190	1300	>5000	>5000	>5000	91	1700	>5000	>5000	>5000
10	330	2900	>5000	>5000	>5000	140	3600	>5000	>5000	>5000

Note: GMB, geomembrane.
*At 95% confidence level. Numbers may not add due to rounding.

the GMB in L5 did not exhibit any decrease in tensile break properties and HLMI over 90 months of immersion, taking into account that the observed Std-OIT depletion time in both solutions at 85 °C was about 2 months. From this comparison, it can be inferred that the presence of salts in the leachate (L3) had a great effect on the time to nominal failure once the antioxidants were depleted. Despite the vertical alignment of the GMB coupons within the jar, salts precipitated onto the GMB surface. This suggests an interaction between the salts and GMB, potentially accelerating the decrease in SCR (Abdelaal et al. 2014*b*).

3.5. Implications for the time to nominal failure in a landfill

The predictions of antioxidant depletion time in Table 3 are for GMBs immersed in simulated MSW leachate L3. It has been demonstrated that the antioxidant depletion time is substantially longer in a composite liner compared to the double-sided leachate immersion method that is used in this study (Rowe and Rimal 2008*a*, 2008*b*; Rimal and Rowe 2009; Rowe et al. 2010, 2013*a*). As explained by Rowe et al. (2020), the depletion times listed in Table 3 can be conservatively multiplied by a composite liner factor of 3.4 to approximate the depletion time in a landfill at a given temperature. One can then add the projected length of stages II and III to get the time to nominal failure, as indicated in Table 5. The procedure is repeated for both the minimum and expected values of the antioxidant depletion time to the "minimum field" and "expected field" times to nominal failure (Table 5) for both the textured and smooth-edge portions of *MxTA15* (Table 5) and for the smooth equivalent roll (Table 6).

Since MSW landfill typically operates in the 35–40 °C temperature range, it is useful to compare results at 40 °C. For the textured portion, the expected t_{NF} is 360 years with a minimum of 280 years. The smooth edge has a notably longer expected t_{NF} of 470 years with a minimum of 360 years. The smooth equivalent roll has an expected t_{NF} of 680 years with a minimum of 590 years. The 320-year difference in expected t_{NF} of 680 years for smooth and 360 years for textured GMB (310-year difference in minimum from 590 years for smooth to 280 years for textured) is significant in many landfill applications.

It follows from the example above that while textured GMBs may be needed on side slopes, they should only be used where the texturing is essential for stability or for health and safety reasons and smooth GMB should be used for the bulk of the project (e.g., the base of landfills or tailings storage facilities). The texturing on the side slopes will likely not be at the same exposure conditions as the base of the landfill where leachate sits and temperatures are the highest. Therefore, the disadvantage of the texturing might even out in the end if placed on the side slopes.

4. Conclusions

The long-term performance of co-extrusion blown-film textured HDPE GMBs (*MxTA15*) relative to its smooth edge and smooth equivalent HDPE GMBs (*MxTsA15* and *MxF15*) was monitored in synthetic MSW leachate (TDS ≈ 12 000 mg/L and pH ≈ 7) at a range of temperatures (40–85 °C) for 8 years to investigate the effect of the texturing. For the test conditions and GMBs examined, it is concluded that

1. For textured and smooth edges, the updated estimates for antioxidant depletion time at four different temperatures (40, 55, 75, and 85 °C), incorporating an additional 60 months of incubation beyond the 34 months reported by Morsy and Rowe (2020*a*), closely align with those estimated by Morsy and Rowe (2020*a*) based on Std-OIT. This suggests that the 34-month test was reasonable for assessing antioxidant depletion when data were well behaved. However, for the smooth equivalent roll, the additional

Table 6. Predicted minimum and expected depletion standard oxidative induction time (Std-OIT) times, $t_{d\ Std\text{-}OIT}$ (years), length of stages II and III ($t_{NF} - t_d$), and predicted minimum and expected time to nominal failure in the field for *MxF15* (rounded to two significant digits) $t_{NF\_Field} = 3.4 * t_{dStd\text{-}OIT} + (t_{NF} - t_d)$.

	MxF15				
Temp. (°C)	Minimum*	Expected	Stages II and III	Minimum $t_{NFfield}$	Expected $t_{NFfield}$
85	0.1	0.2	1.7	2.0	2.4
75	0.4	0.6	5.4	6.7	7.4
65	1.7	1.8	18	24	24
55	4.5	6.1	66	82	87
45	10	21	260	300	330
40	**16**	**42**	**540**	**590**	**680**
35	24	82	1100	1200	1400
30	**39**	**170**	**2400**	**2600**	**3000**
25	62	350	>5000	>5000	>5000
20	100	740	>5000	>5000	>5000
15	170	1600	>5000	>5000	>5000
10	290	3600	>5000	>5000	>5000

*At 95% confidence level. Numbers may not add due to rounding.

Table 7. Predicted times, t_d (years) to OIT depletion (Stage I) from original 34 month Morsy and Rowe (2020*a*) study and this 94-month study.

	MxTA15		*MxTsA15*		*MxF15*	
Temp. (°C)	Morsy and Rowe t_d (years)	This study t_d (years)	Morsy and Rowe t_d (years)	This study t_d (years)	Morsy and Rowe t_d (years)	This study t_d (years)
85	0.2	0.2	0.35	0.3	0.2	0.2
75	0.6	0.6	0.77	0.9	0.6	0.6
65	2	2	1.7	2.5	2	2
55	6	6	8	8	5	6
45	20	20	26	26	16	21
40	**37**	38	49	49	28	42
35	72	74	95	94	53	82
30	**140**	150	190	190	100	170
25	280	300	370	370	200	347
20	**590**	620	760	770	390	740
15	1300	1300	1600	1600	780	1600
10	>2000	>2000	>2000	>2000	1600	>2000

data substantially (by 75%) increased the predicted time to antioxidant depletion due to a change in the antioxidant depletion curve between 30 and 45 months, and this change was not well captured by data up to 34 months.

2. The antioxidants detected by the Std-OIT test depleted significantly faster from the textured portion than from the smooth edge or the smooth equivalent roll.
3. The additional testing was sufficient for nominal failure to be reached at 75 °C after 6 years of immersion in the simulated MSW leachate. These data combined with those for nominal failure at 85°C provide the first opportunity to predict the time between depletion of Std-OIT and nominal failure at lower temperatures. Based on this information, the expected time to nominal failure at 40° C in an MSW landfill is 360 years (textured), 470 years (smooth edge), and 680 years (smooth equivalent).
4. The textured part of the GMB exhibited increased variability in thickness, resulting in lower break properties and a faster degradation rate compared to the smooth edges. This can be attributed to stress concentrations between the asperities, contributing to significant variability in the break properties of the textured GMBs with aging.
5. Based on the information in this paper, the use of textured GMB should be restricted to those locations where it is needed, and smooth GMB should be used elsewhere.
6. GMB *MxTA15* was immersed in two simulated MSW leachates with surfactant and trace metals denoted L5 and L3. These leachates were identical except that L3 also had concentrations of salts, giving a total dissolved solids of 12 000 mg/L. The GMB in the two solutions had similar Std-OIT depletion time, but the GMB immersed in L3 reached nominal failure based on SCR after 28 months at 85 °C and had experienced a decrease in tensile break properties and melt index. In contrast, the same GMB immersed in L5 had SCR equal to 1390 ± 890 h after 90 months and did not exhibit any decrease in tensile break properties or

melt index over 90 months of immersion in L5. It is inferred that the salts played a pivotal role in the difference in behaviour.

This study focused on a double-sided textured GMB, and it is recommended to explore different textured GMB products with varying thicknesses and asperities for a comprehensive understanding.

Acknowledgements

The research presented in this paper was supported by the Natural Sciences and Engineering Council of Canada (NSERC Discovery Grant RGPIN/03928-2022). The equipment used was provided by funding from the Canada Foundation for Innovation (CFI) and the Government Ontario's Ministry of Research and Innovation.

Article information

History dates

Received: 11 January 2024
Accepted: 12 March 2024
Accepted manuscript online: 8 April 2024
Version of record online: 29 November 2024

Copyright

Data availability

Some or all data used are available from the corresponding author by request.

Author information

Author ORCIDs

R. Kerry Rowe https://orcid.org/0000-0002-1009-0447

Author notes

R. Kerry Rowe served as an Associate Editor at the time of manuscript review and acceptance; peer review and editorial decisions regarding this manuscript were handled by another Editorial Board Member.

Author contributions

Conceptualization: RKR
Data curation: RKR, MMA
Formal analysis: RKR, MSM
Funding acquisition: RKR
Investigation: RKR, MMA, MSM
Methodology: RKR, MSM
Project administration: RKR
Resources: RKR
Supervision: RKR
Validation: RKR, MMA
Writing – original draft: MMA
Writing – review & editing: RKR, MSM

Competing interests

The authors declare there are no competing interests.

Supplementary material

Supplementary data are available with the article at https://doi.org/10.1139/cgj-2024-0024.

References

Abdelaal, E.B., Zafai, M., and Rowe, R.K. 2023*b*. Assessment of the stress crack resistance of multilayered textured HDPE geomembranes. Geosynthetics International, 1–15. doi:10.1680/jgein.23.00096.

Abdelaal, F.B., and Rowe, R.K. 2014. Effect of high temperatures on antioxidant depletion from different HDPE geomembranes. Geotextiles and Geomembranes, **42**: 284–301. doi:10.1016/j.geotexmem.2014.05.002.

Abdelaal, F.B., and Rowe, R.K. 2017. Effect of high pH found in low-level radioactive waste leachates on the antioxidant depletion of a HDPE geomembrane. Journal of Hazardous, Toxic, and Radioactive Waste, **21**: D4015001. doi:10.1061/(ASCE)HZ.2153-5515.0000262.

Abdelaal, F.B., Morsy, M.S., and Rowe, R.K. 2019. Long-term performance of a HDPE geomembrane stabilized with HALS in chlorinated water. Geotextiles and Geomembranes, **47**: 815–830. doi:10.1016/j.geotexmem.2019.103497.

Abdelaal, F.B., Rowe, R.K., and Brachman, R.W.I. 2014*a*. Brittle rupture of an aged HPDE geomembrane at local gravel indentations under simulated field conditions. Geosynthetics International, **21**: 1–23. doi:10.1680/gein.13.00031.

Abdelaal, F.B., Rowe, R.K., and Islam, M.Z. 2014*b*. Effect of leachate composition on the long-term performance of a HDPE geomembrane. Geotextiles and Geomembranes, **42**: 348–362. doi:10.1016/j.geotexmem.2014.06.001.

Abdelaal, F.B., Rowe, R.K., Morsy, M.S., and Silva, R.A.E. 2023*a*. Degradation of HDPE, LLDPE, and blended polyethylene geomembranes in extremely low and high pH mining solutions at 85 °C. Geotextiles and Geomembranes, **51**: 27–38. doi:10.1016/j.geotexmem.2023.04.011.

Abdelaal, F.B., Zafari, M., and Rowe, R.K. 2023. Assessment of the stress crack resistance of multilayered textured HDPE geomembranes. Geosynthetics International, ISSN 1072-6349. doi:10.1680/jgein.23.00096.

Arrhenius, S.A. 1889a. Über die Dissociationswärme und den Einfluß der Temperatur auf den Dissociationsgrad der Elektrolyte. Zeitschrift für Physikalische Chemie, **4U**: 226–248. doi:10.1515/zpch-1889-0416. S2CID 100032801.

Arrhenius, S.A. 1889b. Über die Reaktionsgeschwindigkeit bei der Inversion von Rohrzucker durch Säuren. Zeitschrift für Physikalische Chemie, **4U**: 226–248. Available from zenodo.org/records/1749766. doi:10.1515/zpch-1889-0416.

ASTM 2010a. Standard test method for measuring core thickness of textured geomembranes. American society for testing and materials. West Conshohocken, PA, USA. D5994.

ASTM 2010b. Standard test method for measuring asperity height of textured geomembranes. American society for testing and materials. West Conshohocken, PA, USA. D7466.

ASTM 2010c. Standard test method for density of plastics by the density-gradient technique. American society for testing and materials. West Conshohocken, PA. D1505.

ASTM. 2012. Standard method for measuring the nominal thickness of geosynthetics. American Society for Testing and Materials. West Conshohocken, PA. D5199.

ASTM. 2013. Standard test method for melt flow rates of thermoplastics by extrusion plastometer. American society for testing and materials. West Conshohocken, Pennsylvania, USA. D1238.

ASTM. 2014. Standard test method for tensile properties of plastics D638. American Society for testing and materials. West Conshohocken, Pennsylvania, USA.

ASTM. 2019. Standard test method for oxidative induction time of polyolefins by differential scanning calorimetry D3895. American Society for Testing and Materials, West Conshohocken, Pennsylvania, USA.

ASTM. 2020a. Standard test method for evaluation of stress crack resistance of polyolefin geomembranes using notched constant tensile load test. ASTM International, West Conshohocken, PA,USA. D5397.
ASTM. 2020b. Standard test method for determining tensile properties of nonreinforced polyethylene and nonreinforced flexible polypropylene geomembranes D6693, ASTM International, West Conshohocken, PA, USA.
ASTM. 2020c. Standard test method for oxidative induction time of polyolefin geosynthetics by high-pressure differential scanning calorimetry. ASTM D5885. ASTM, West Conshohocken, PA.
ASTM. 2021. Standard test method for oxidative induction time of polyolefin geosynthetics by differential scanning calorimetry D8117. American Society for Testing and Materials, West Conshohocken, Pennsylvania, USA.
Chaoui, K., Chudnovsky, A., and Moet, A. 1987. Effect of residual stress on crack propagation in MDPE pipes. Journal of Materials Science, **22**(11): 3873–3879. doi:10.1007/BF01133334.
Clinton, M., and Rowe, R.K. 2023. Long-term durability of two HDPE geomembranes formulated with polyethylene of raised temperature resistance (PE-RT). Geotextiles and Geomembranes, **52**(3) 304–318.
Erickson, R.B., Thiel, R.S., and Peters, J. 2008. The ongoing quality issues regarding polyethylene geomembrane material manufacturing and installation. *In* Proceedings of the First Pan American Geosynthetics Conference and Exhibition, 2–5 March 2008, Cancun, Mexico.
Ewais, A.M.R., and Rowe, R.K. 2014. Effect of aging on the stress crack resistance of an HDPE geomembrane. Polymer Degradation and Stability, **109**: 194–208. doi:10.1016/j.polymdegradstab.2014.06.013.
Ewais, A.M.R., Rowe, R.K., and Scheirs, J. 2014. Degradation behavior of HDPE geomembranes with high and low initial high-pressure oxidative induction time. Geotextiles and Geomembranes, **42**(Jun): 111–126. doi:10.1016/j.geotexmem.2014.01.004.
Ewais, A.M.R., Rowe, R.K., Rimal, S., and Sangam, H.P. 2018. 17-year elevated temperature study of HDPE geomembrane longevity in air, water and leachate. Geosynthetics International, **25**: 525–544. doi:10.1680/jgein.18.00016.
Giroud, J.P., and Bonaparte, R. 1989. Leakage through liners constructed with geomembranes. 1. Geomembrane liners. Geotextiles and Geomembranes, **8**: 27–67. doi:10.1016/0266-1144(89)90009-5.
GRI-GM13. 2019. Standard specification for test methods, test properties, and testing frequency for high density polyethylene (HDPE) smooth and textured geomembranes. Geosynthetic Research Institute, Pennsylvania, USA.
Hsuan, Y., Schroeder, H., Rowe, K., Müller, W., Greenwood, J., Cazzuffi, D., and Koerner, R.M. 2008. Long-term performance and lifetime prediction of geosynthetics. Proceedings of the 4th European Conference on Geosynthetics, Edinburgh, September. Keynote paper.
Hsuan, Y.G., and Koerner, R.M. 1998. Antioxidant depletion lifetime in high density polyethylene geomembranes. Journal of Geotechnical and Geoenvironmental Engineering, **124**: 532–541. doi:10.1061/(ASCE)1090-0241(1998)124:6(532).
Koerner, R.M. 2005. Designing with geosynthetics. 5th ed. Pearson Prentice hall.
Koerner, R.M., Lord, A.E., and Hsuan, Y.H. 1992. Arrhenius modeling to predict geosynthetic degradation. Geotextiles and Geomembranes, **11**: 151–183. doi:10.1016/0266-1144(92)90042-9.
Morsy, M.S., and Rowe, R.K. 2017. Effect of texturing on antioxidant depletion rate from HDPE geomembranes. *In* Proceedings of the 19th International Conference on Soil Mechanics and Geotechnical Engineering. Seoul, South Korea. pp. 3175–3178.
Morsy, M.S., and Rowe, R.K. 2020a. Effect of texturing on the longevity of high-density polyethylene (HDPE) geomembranes in municipal solid waste landfills. Canadian Geotechnical Journal, **57**: 61–72. doi:10.1139/cgj-2019-0047.
Morsy, M.S., and Rowe, R.K. 2020b. Stress crack-resistance of textured geomembranes. *In* Pan American Conference on Geosynthetics. pp. 1–6.
Morsy, M.S., Rowe, R.K., and Abdelaal, F.B. 2021. Longevity of 12 geomembranes in chlorinated water. Canadian Geotechnical Journal, **58**: 479–495. doi:10.1139/cgj-2019-0520.
Mueller, W., and Jakob, I. 2003. Oxidative resistance of high-density polyethylene geomembranes. Polymer Degradation and Stability, **79**: 161–172. doi:10.1016/S0141-3910(02)00269-0.
Müller, W.W. 2007. HDPE geomembranes in geotechnics. Springer, Berlin.
Rimal, S., and Rowe, R.K. 2009. Diffusion modelling of OIT depletion from HDPE geomembrane in landfill applications. Geosynthetics International **16**(3): 183–196. doi:10.1680/gein.2009.16.3.183.
Rowe, R.K. 2005. Long-term performance of contaminant barrier systems. Géotechnique, **55**: 631–678. doi:10.1680/geot.2005.55.9.631.
Rowe, R.K. 2020. Protecting the environment with geosynthetics: 53rd Karl Terzaghi lecture. Journal of Geotechnical and Geoenvironmental Engineering, **146**: 04020081. doi:10.1061/(ASCE)GT.1943-5606.0002239.
Rowe, R.K., Abdelaal, F.B., and Brachman, R.W.I. 2013. Antioxidant depletion of HDPE geomembrane with sand protection layer. Geotextiles and Geomembranes, **27**(2): 137–151.
Rowe, R.K., Abdelaal, F.B., Zafari, M., Morsy, M.S., and Priyanto, D.G. 2020. An approach to high-density polyethylene (HDPE) geomembrane selection for challenging design requirements. Canadian Geotechnical Journal, **57**: 1550–1565. doi:10.1139/cgj-2019-0572.
Rowe, R.K., and Ewais, A.M.R. 2014. Antioxidant depletion from five geomembranes of same resin but of different thicknesses immersed in leachate. Geotextiles and Geomembranes, **42**: 540–554. doi:10.1016/j.geotexmem.2014.08.001.
Rowe, R.K., and Rimal, S. 2008a. Depletion of antioxidants from an HDPE geomembrane in a composite liner. ASCE Journal of Geotechnical and Geoenvironmental Engineering, **134**(1): 68–78.
Rowe, R.K., and Rimal, S. 2008b. Ageing of HDPE geomembrane in three composite liner configurations. Journal of Geotechnical and Geoenvironmental Engineering, **134**(7): 906–916. doi:10.1061/(ASCE)1090-0241(2008)134:7(906).
Rowe, R.K., and Sangam, H.P. 2002. Durability of HDPE geomembranes. Geotextiles and Geomembranes, **20**: 77–95.
Rowe, R.K., and Shoaib, M. 2017. Effect of brine on long-term performance of four HDPE geomembranes. Geosynthetics International, **24**: 508–523. doi:10.1680/jgein.17.00018.
Rowe, R.K., and Somuah, M. 2023. Effects of perfluoroalkyl substances (PFAS) on antioxidant depletion from a high-density polyethylene geomembrane. Journal of Environmental Management, **328**: 116979. doi:10.1016/j.jenvman.2022.116979.
Rowe, R.K., Hsuan, Y.G., Lake, C.B., Sangam, P., and Usher, S. 1998. Evaluation of a composite (geomembrane/clay) liner for a lagoon after 14 years of use. *In* Proceedings of the 6th International Conference on Geosynthetics. Atlanta. pp. 191–196.
Rowe, R.K., Islam, M.Z., and Hsuan, Y.G. 2008. Leachate chemical composition effects on OIT depletion in an HDPE geomembrane. Geosynthetics International, **15**: 136–151. doi:10.1680/gein.2008.15.2.136.
Rowe, R.K., Islam, M.Z., Brachman, R.W.I., Arnepalli, D.N., and Ewais, A.R. 2010. Antioxidant depletion from an HDPE geomembrane under simulated landfill conditions. Journal of Geotechnical and Geoenvironmental Engineering, **136**:(7): 930–939. doi:10.1061/(ASCE)GT.1943-5606.0000302.
Rowe, R.K., Morsy, M.S., and Ewais, A.M.R. 2019. Representative stress crack resistance of polyolefin geomembranes used in waste management. Waste Management, **100**: 18–27. doi:10.1016/j.wasman.2019.08.028.
Rowe, R.K., Quigley, R.M., Brachman, R.W.I., and Brachman, R.W.I. 2004. Barrier Systems for waste disposal facilities. 2nd ed. Spon Press, New York, USA.
Rowe, R.K., Rimal, S., and Sangam, H. 2009. Ageing of HDPE geomembrane exposed to air, water and leachate at different temperatures. Geotextiles and Geomembranes, **27**: 137–151. doi:10.1016/j.geotexmem.2008.09.007.
Sangam, H.O., and Rowe, R.K. 2002. Effects of exposure conditions on the depletion of antioxidants from high-density polyethylene (HDPE) geomembranes. Canadian Geotechnical Journal, **39**: 1221–1230. doi:10.1139/t02-074.
Scheirs, J. 2009. A guide to polymeric geomembranes: a practical approach. John Wiley & Sons.
Scheirs, J., Marta, A.L., Armstrong, C.J., and Jotani, R. 2020. Rapid screening test for assessing durability of geomembranes in mining liquors. GeoAmericas, Rio De Janeiro, Brazil.
Tian, K., Benson, C.H., Tinjum, J.M., and Edil, T.B. 2017. Antioxidant depletion and service life prediction for HDPE geomembranes exposed

to low-level radioactive waste leachate. Journal of Geotechnical and Geoenvironmental Engineering, 143.

Xu, H., and Bellehumeur, C.T. 2008. Thermal residual stress development for semi-crystalline polymers in rotational molding. Polymer Engineering & Science, **48**(2): 283–291.

Zafari, M., Abdelaal, F.B., and Rowe, R.K. 2023a. Degradation behavior of two multilayered textured white HDPE geomembranes and their smooth edges. Journal of Geotechnical and Geoenvironmental Engineering, 149.

Zafari, M., Abdelaal, F.B., and Rowe, R.K. 2023b. Long-term performance of conductive-backed multi-layered HDPE geomembranes, Geotextiles and Geomembranes, **51**(4): 137–155. doi:10.1016/j.geotexmem.2023.03.007.

Zafari, M., Rowe, R.K., and Abdelaal, F.B. 2024. Longevity of multi-layered textured HDPE geomembranes in low-level waste applications. Canadian Geotechnical Journal, **61**: 684–699. In press. doi:10.1139/cgj-2023-0039.